Calhoun: The NPS Institutional Archive
DSpace Repository

Theses and Dissertations 1. Thesis and Dissertation Collection, all items

1977-06

Divergent initialization experiments using a global primitive equation spectral model

Lubeck, Olaf Martin

Monterey, California. Naval Postgraduate School

http://hdl.handle.net/10945/18087

This publication is a work of the U.S. Government as defined in Title 17, United States Code, Section 101. Copyright protection is not available for this work in the United States.

Downloaded from NPS Archive: Calhoun

Calhoun is the Naval Postgraduate School's public access digital repository for research materials and institutional publications created by the NPS community. Calhoun is named for Professor of Mathematics Guy K. Calhoun, NPS's first appointed -- and published -- scholarly author.

Dudley Knox Library / Naval Postgraduate School
411 Dyer Road / 1 University Circle
Monterey, California USA 93943

http://www.nps.edu/library

DIVERGENT INITIALIZATION EXPERIMENTS USING A GLOBAL PRIMITIVE EQUATION SPECTRAL MODEL

Olaf Martin Lubeck

LIBRARY
NAVAL POSTGRADUATE SCHOOL

DUDLEY KNOX LIBRARY

NAVAL POSTGRADUATE SCHOOL
Monterey, California

THESIS

DIVERGENT INITIALIZATION
EXPERIMENTS USING A GLOBAL PRIMITIVE
EQUATION SPECTRAL MODEL

by

Olaf Martin Lubeck

June 1977

Thesis Advisor: R. T. Williams

Approved for public release; distribution unlimited.

T180093

REPORT DOCUMENTATION PAGE

READ INSTRUCTIONS
BEFORE COMPLETING FORM

1. REPORT NUMBER	2. GOVT ACCESSION NO.	3. RECIPIENT'S CATALOG NUMBER

4. TITLE (and Subtitle)
Divergent Initialization Experiments Using a Global Primitive Equation Spectral Model

5. TYPE OF REPORT & PERIOD COVERED
Master's Thesis:
June 1977

6. PERFORMING ORG. REPORT NUMBER

7. AUTHOR(s)
Olaf Martin Lubeck

8. CONTRACT OR GRANT NUMBER(s)

9. PERFORMING ORGANIZATION NAME AND ADDRESS
Naval Postgraduate School
Monterey, California 93940

10. PROGRAM ELEMENT, PROJECT, TASK AREA & WORK UNIT NUMBERS

11. CONTROLLING OFFICE NAME AND ADDRESS
Naval Postgraduate School
Monterey, California 93940

12. REPORT DATE
June 1977

13. NUMBER OF PAGES
76

14. MONITORING AGENCY NAME & ADDRESS (if different from Controlling Office)
Naval Postgraduate School
Monterey, California 93940

15. SECURITY CLASS. (of this report)
Unclassified

15a. DECLASSIFICATION/DOWNGRADING SCHEDULE

16. DISTRIBUTION STATEMENT (of this Report)

Approved for public release; distribution unlimited.

17. DISTRIBUTION STATEMENT (of the abstract entered in Block 20, if different from Report)

18. SUPPLEMENTARY NOTES

19. KEY WORDS (Continue on reverse side if necessary and identify by block number)

20. ABSTRACT (Continue on reverse side if necessary and identify by block number)

An initialization of a spectral formulation of the primitive equations using a diagnostic divergence is tested for a global model. The initial conditions are generated from a developing baroclinically unstable wave. A semi-implicit time scheme is

DD FORM 1 JAN 73 1473 EDITION OF 1 NOV 65 IS OBSOLETE
S/N 0102-014-6601 |

developed and tested along with the usual explicit method during the course of the experiments. Results show a relatively small effect of a divergent initialization on the ensuing integrations. The semi-implicit method shows a tendency to smooth out high frequency oscillations in local tendencies.

Approved for public release; distribution unlimited.

Divergent Initialization Experiments Using a Global Primitive Equation Spectral Model

by

Olaf Martin Lubeck
Lieutenant, United States Navy
B.A., University of Colorado, 1971

Submitted in partial fulfillment of the
requirements for the degree of

MASTER OF SCIENCE IN METEOROLOGY

from the

NAVAL POSTGRADUATE SCHOOL
June 1977

Thesis
L885
c.1

ABSTRACT

An initialization of a spectral formulation of the primitive equations using a diagnostic divergence is tested for a global model. The initial conditions are generated from a developing baroclinically unstable wave. A semi-implicit time scheme is developed and tested along with the usual explicit method during the course of the experiments. Results show a relatively small effect of a divergent initialization on the ensuing integrations. The semi-implicit method shows a tendency to smooth out high frequency oscillations in local tendencies.

NAVAL

TABLE OF CONTENTS

I. INTRODUCTION - 10

II. MODEL DESCRIPTION - - - - - - - - - - - - - - - - - - 12

III. SEMI-IMPLICIT SCHEME - - - - - - - - - - - - - - - - - 20

IV. QUASI-GEOSTROPHIC DIVERGENCE - - - - - - - - - - - - 23

V. DESIGN OF THE EXPERIMENTS - - - - - - - - - - - - - 29

VI. RESULTS - 32

- A. CONTROL CASE - - - - - - - - - - - - - - - - - - - 32
- B. GRAVITY WAVES - - - - - - - - - - - - - - - - - - 41
- C. EXPERIMENTS A AND B - - - - - - - - - - - - - - - 48
  - 1. Low Resolution - - - - - - - - - - - - - - - - 48
  - 2. High Resolution - - - - - - - - - - - - - - - 56
- D. EXPERIMENT C - - - - - - - - - - - - - - - - - - - 67

VII. SUMMARY AND CONCLUSIONS - - - - - - - - - - - - - - - 73

REFERENCES - 75

INITIAL DISTRIBUTION LIST - - - - - - - - - - - - - - - - - 76

LIST OF FIGURES

1. Staggered 5-layer sigma coordinate system - - - - 16

2. Vorticity time series during the first 192 hrs. Vertical axis is logarithmic. Units are $secs^{-1}$. Solid curve is the magnitude of wave no. 0 at latitude 60°N. Dotted curve is $m=6$, short dashes are $m=12$ and long dashes are $m=18$ - - - - - - - - - - - - 30

3. Initial low resolution surface pressure. Contour interval is 5 mb - - - - - - - - - - - - - - 33

4. Initial low resolution temperature for $\sigma = .9$. Contour interval is 5°K - - - - - - - - - - 34

5. Initial low resolution vorticity for $\sigma = .9$. Contour interval is $5 \times 10^{-6} sec^{-1}$. Mean field is scaled by 10^6 - - - - - - - - - - - - - 35

6. Initial low resolution divergence for $\sigma = .9$. Contour interval is $1 \times 10^{-6} sec^{-1}$. Mean field is scaled by 10^6 - - - - - - - - - - - - - 36

7. Initial high resolution surface pressure. Contour interval is 5 mb - - - - - - - - - - - - - - 37

8. Initial high resolution temperature for $\sigma = .9$. Contour interval is 5°K - - - - - - - - - - 38

9. Initial high resolution vorticity for $\sigma = .9$. Contour interval is $5 \times 10^{-6} sec^{-1}$. Mean field is scaled by 10^6 - - - - - - - - - - - - - 39

10. Initial high resolution divergence for $\sigma = .9$. Contour interval is $1 \times 10^{-6} sec^{-1}$. Mean field is scaled by 10^6 - - - - - - - - - - - - - 40

11. 12 hr high resolution temperature for $\sigma = .9$. Contour interval is 5°K - - - - - - - - - - 42

12. 24 hr high resolution temperature for $\sigma = .9$. Contour interval is 5°K - - - - - - - - - - 43

13. 36 hr high resolution temperature for $\sigma = .9$. Contour interval is 5°K - - - - - - - - - - 44

14. 72 hr high resolution temperature for $\sigma = .9$. Contour interval is 5°K - - - - - - - - - - 45

15. 72 hr low resolution temperature for $\sigma = .9$. Contour interval is 5°K - - - - - - - - - - 46

16. Structure and eigenvelocities of the external and four internal divergence modes. Velocities are in m/sec - - - - - - - - - - - 47

17. Divergence time series of the external mode for the low resolution control case. Vertical axis units are $\sec^{-1}$. Time is in hrs - 49

18. Time series of the first internal mode - otherwise as in Fig. 17 - - - - - - - - - - - - - - 50

19. $\partial q/\partial t$ for a low resolution Experiment A (19a), Experiment B (19b) and the control case (19c). Time is in hrs. Vertical scale is $\sec^{-1}$ - 51

20. Gravity wave noise in the external mode for low resolution Experiment A (20a) and Experiment B (20b). Vertical scale is $\sec^{-1}$. Time is in hrs - - - - - - - - - - - - - - 53

21. Gravity wave noise in the first internal mode - otherwise as in Fig. 20 - - - - - - - - - - - 54

22. Gravity wave noise in the second internal mode - otherwise as in Fig. 20 - - - - - - - - - - - 55

23. Quasi-geostrophic divergence (high resolution) for $\sigma = .9$. Contour interval is $1 \times 10^{-6} \sec^{-1}$. Mean field is scaled by 10^6 - - 57

24. Gravity wave noise in the external mode for high resolution Experiment A (24a) and Experiment B (24b). Vertical scale is $\sec^{-1}$. Time is in hrs - - - - - - - - - - - - - - - 58

25. Gravity wave noise in the first interval mode - otherwise as in Fig. 24 - - - - - - - - - - - 59

26. Gravity wave noise in the second interval mode - otherwise as in Fig. 24 - - - - - - - - - - - 60

27. Initial divergence coefficients for the control case (dotted line) and Experiment B (dashed line). Vertical axis is latitudinal wave number (lat. index of the spherical harmonics). Horizontal scale is $\sec^{-1}$ - - - - - - 61

28. 6 hr divergence coefficients for the control case (dotted line) and Experiment A (dashed line) - otherwise as in Fig. 27 - - - - - - 63

29. 6 hr divergence coefficients for the control case (dotted line) and Experiment B (dashed line) - otherwise as in Fig. 27 - - - - - - 64

30. Time series of the gravity wave noise in the modified Experiment B. Vertical scale is $\sec^{-1}$. Time is in hrs - - - - - - - - - - - - - - 65

31. 6 hr divergence coefficients for the control case (dotted line) and modified Experiment B (dashed line). Vertical axis latitudinal wave no. Horizontal scale is $\sec^{-1}$ - - - - - - - - 66

32. $\partial q/\partial t$ for Experiment C with a time step of 12 mins (32a) and 60 mins (32b). Vertical scale is $\sec^{-1}$ - 69

33. Gravity wave noise in the external mode for Experiment C with time steps of 12 mins (33a) and 60 mins (33b). Vertical scale is $\sec^{-1}$ - 70

34. 3 hr divergence coefficients for the low resolution control case (dotted line) and Experiment C with a 12 min time step (dashed line). Vertical axis is latitudinal wave no. Horizontal scale is $\sec^{-1}$ - - - - - - - - 71

35. 3 hr divergence coefficients with a 60 min time step - otherwise as in Fig. 34 - - - - - - - - 72

ACKNOWLEDGEMENTS

The author would like to thank Dr. R. T. Williams for his insight, suggestions and overall guidance during the course of this thesis. Dr. T. Rosmond graciously provided the spectral model used in the experiments and many fruitful discussions with him resulted in valuable contributions to this thesis. Dr. G. J. Haltiner reviewed the results and manuscript and added many helpful suggestions. The calculations were performed using the computer facilities of Fleet Numerical Weather Central. Finally, the author wishes to thank his wife whose encouragement never ended throughout the period of his graduate studies at the Naval Postgraduate School.

I. INTRODUCTION

The emphasis of this thesis is two-fold. The first point is to gain insight into the characteristics of a spectral primitive equation model. The second is to attempt to take advantage of the spectral expansions in an initialization technique.

A spectral model uses a Galerkin formulation with the spherical harmonics as its choice of basis functions. The basis functions are eigenfunctions of the Laplacian operator in spherical geometry and, thus, are used to advantage for global integrations. An immediate consequence of the Galerkin formulation is that spatial derivatives of a single wave are computed without the usual truncation error present in finite difference methods. This means that the spectral model contains no linear phase speed errors.

The non-linear terms are computed via a transform grid in physical space (Orszag, 1971). This procedure is responsible for making the efficiency of the spectral model comparable with finite difference methods. In addition, the non-linear terms may be computed without aliasing. This prevents non-linear instability and conserves invariant integral properties. Physical processes are also computed on the transform grid.

The second objective of this thesis is to test a divergent initialization for the spectral model. Most static and

NAVAL

variational initialization techniques of global primitive equation models use a constraint to balance the rotational part of the wind with the mass field while setting the divergent part to zero. Phillips (1960) has shown that a completely non-divergent initialization cannot eliminate the gravity waves which would be generated and his work suggests that the quasi-geostrophic divergence could tend to suppress these gravity wave modes for mid-latitude synoptic scales. In addition, if the quasi-geostrophic divergence had internal modes close to those which would be developed by the model, such things as the large scale precipitation would be more realistic during the first few hours of the model forecast.

It is an aim of this thesis to develop a diagnostic velocity divergence to insert into the fields of an otherwise completely balanced system and to test the subsequent effect on the spurious gravity wave noise and the developing divergence.

A spectral formulation of the primitive equations can lend itself to techniques which initialize according to scale. For example, the quasi-geostrophic divergence might be computed only for the synoptic scales of the model. Furthermore, the model conveniently supplies diagnostic information about the various scales.

The final goal of this thesis is to develop a semi-implicit time differencing scheme and test its effects during the first few model hours after initialization.

AVAL

II. MODEL DESCRIPTION

The model described here has been developed by Rosmond (1977) and the details are presented here for reference purposes. Similar formulations have been done by Hoskins and Simmons (1975) and by Bourke (1974). The equations for an inviscid, adiabatic and hydrostatic atmosphere may be written as

$$\text{I.1)} \quad \frac{\partial \zeta}{\partial t} = -\nabla \cdot (\zeta + f)\vec{V} - \hat{k} \cdot \nabla \times (RT\nabla q + \dot{\sigma} \frac{\partial \vec{V}}{\partial \sigma})$$

$$\text{I.2)} \quad \frac{\partial D}{\partial t} = \hat{k} \cdot \nabla \times (\zeta + f)\vec{V} - \nabla \cdot (RT\nabla q + \dot{\sigma} \frac{\partial \vec{V}}{\partial \sigma}) - \nabla^2 (\phi + \frac{\vec{V}^2}{2})$$

$$\text{I.3)} \quad \frac{\partial \theta}{\partial t} = -\vec{V} \cdot \nabla \theta - \sigma \frac{\partial \theta}{\partial \sigma}$$

$$\text{I.4)} \quad \frac{\partial q}{\partial t} = -D - \vec{V} \cdot \nabla q - \frac{\partial \dot{\sigma}}{\partial \sigma}$$

$$\text{I.5)} \quad \sigma \frac{\partial \phi}{\partial \sigma} = -RT$$

where

ζ - vorticity ($\zeta = \hat{k} \cdot \nabla \times \vec{V}$)

D - velocity divergence ($D = \nabla \cdot \vec{V}$)

T - temperature

θ - potential temperature

π - surface pressure

$\vec{V}$ - horizontal velocity vector

ϕ - geopotential height

R - gas constant

C_p - specific heat

NAVAL

f - Coriolis parameter

σ - vertical coordinate ($\sigma = p/\pi$)

$\dot{\sigma}$ - vertical velocity ($\dot{\sigma} = d\sigma/dt$)

q - $\ln\pi$

The continuity equation (1.4) may be refined by integrating in the vertical and imposing boundary conditions on $\dot{\sigma}$; $\dot{\sigma}(0) = \dot{\sigma}(1) = 0$. Introducing the notation $G = \vec{V}\cdot\nabla q$, we may rewrite Eq. (1.4) as

$$1.6)\quad \frac{\partial q}{\partial t} = -(\bar{D} + \bar{G}) \ .$$

where the over bar denotes a vertical average.

The vertical velocity, $\dot{\sigma}$, may be obtained diagnostically by substituting Eq. (1.6) into Eq. (1.4) and integrating in the vertical to obtain

$$1.7)\quad \dot{\sigma} = (\bar{D} + \bar{G})\sigma - \int_0^{\sigma} (G + D)\, d\sigma \ .$$

By defining a horizontally mean temperature,

$$T = T^*(\sigma) + T'(\sigma, \lambda, \theta, t)$$

and using the following operator

$$\alpha(X,Y) = \frac{1}{1-\mu^2}\frac{\partial X}{\partial \lambda} + \frac{\partial Y}{\partial \mu}$$

NAVAL

We can now expand the vector quantities in our basic equations in spherical coordinates (λ,η) to arrive at

$$1.8)\quad \frac{\partial\zeta}{\partial t} = -\alpha(A,B)$$

$$1.9)\quad \frac{\partial D}{\partial t} = \alpha(B,-A) - \nabla^2(r^2 E + \phi + RT^* q)$$

$$1.10)\quad \frac{\partial\theta}{\partial t} = -\alpha(U\theta,V\theta) + \theta D - \dot{\sigma}\frac{\partial\theta}{\partial\sigma}$$

$$1.11)\quad \frac{\partial q}{\partial t} = -(\bar{D} + \bar{G})$$

$$1.12)\quad \sigma\frac{\partial\phi}{\partial\sigma} = -RT$$

where

$$A = (\zeta+f)U + \dot{\sigma}\frac{\partial V}{\partial\sigma} + \frac{RT'}{r^2}\cos\theta$$

$$B = (\zeta+f)V - \dot{\sigma}\frac{\partial U}{\partial\sigma} - \frac{RT'}{r^2}\frac{\partial \ell n\pi}{\partial\lambda}$$

$$G = \frac{U}{1-\mu^2}\frac{\partial \ell n\pi}{\partial\lambda} + V\frac{\partial \ell n\pi}{\partial\mu}$$

$$E = \frac{U^2 + V^2}{2(1-\mu^2)}$$

$U = u\cos\eta/r$

$V = v\cos\eta/r$

λ = longitude

η = latitude

$\mu = \sin\eta$

Equations (1.8) - (1.12) are the basic equations used in the model. The equations are represented spectrally in the horizontal and finite differenced in the vertical. The dependent variables are written in terms of a triangularly truncated series of spherical harmonics:

$$X = \Sigma X_\ell^m \quad Y_\ell^m$$

where the summation is a double sum over m,n for $|m| \leq M$ and $|m| \leq \ell \leq M$. The separation is such that the coefficients, X_ℓ^m, are functions of time and vertical coordinate and the spherical harmonics, Y_ℓ^m, are horizontal functions of space. The normalization and orthogonality properties of the Y_ℓ^m allow the coefficients to be obtained as follows:

$$X_\ell^m = \langle X, \ Y_\ell^m \rangle \equiv \frac{1}{4\pi} \int_0^{2\pi} \int_{-1}^{+1} X \, Y_\ell^m \, d\mu d\lambda \ .$$

The model used for this study has five vertical layers staggered as in Fig. 1. The even levels carry $\dot{\sigma}$ and the odd levels carry all the dependent variables plus the diagnostic variables, U,V.

The finite difference scheme for the vertical advection terms is

$$\dot{\sigma} \frac{\partial X}{\partial \sigma} = \frac{1}{2(\Delta\sigma_k)} [(X_{k+1} - X_k)\dot{\sigma}_{k+1} + (X_k - X_{k-1})\dot{\sigma}_k].$$

This formulation conserves kinetic energy.

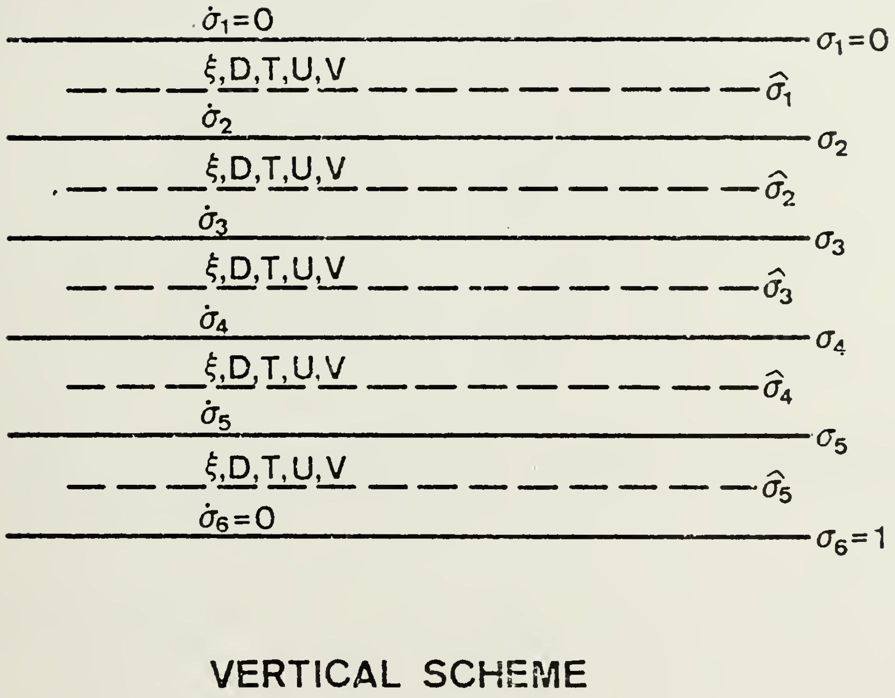

Figure 1. Staggered 5-layer sigma coordinate system.

Following Arakawa and Lamb (1976), the hydrostatic equation (1.12) can be finite differenced as

1.13) $$\phi_{k+1} - \phi_k = - \frac{C_p}{2} (\alpha_k T_{k+1} + \beta_k T_k)$$

where

$$\alpha_k = 1 - (\hat{\sigma}_k / \hat{\sigma}_{k+1})^{R/C_p} \quad \text{and} \quad \beta_k = (\hat{\sigma}_{k+1} / \hat{\sigma}_k)^{R/C_p} - 1 \,.$$

A boundary condition is formed by integrating the hydrostatic equation from $\sigma = 0$ to 1 which gives

$$\int_0^1 \sigma \frac{\partial \phi}{\partial \sigma} d\sigma = -R \int_0^1 T \, d\sigma$$

or

$$\int_0^1 \phi d\sigma - \phi_{sfc} = R \int_0^1 T \, d\sigma$$

where ϕ_{sfc} is the terrain geopotential. This boundary condition is then finite differenced as

1.14) $$\sum_k \phi_k (\Delta\sigma_k) - \phi_{sfc} = R \sum T_k (\Delta\sigma_k)$$

Equations (1.13) and (1.14) are then combined to give the matrix equation

1.15) $$\phi = [C] T + \phi_{sfc}$$

which is the finite difference form of the hydrostatic equation where the variables are now column vectors.

NAVAL

The pressure tendency equation (1.11) can be written as

$$\frac{\partial q}{\partial t} = - \sum_k (G_k + D_k)(\Delta\sigma_k)$$

or in matrix form as

1.16) $$\frac{\partial q}{\partial t} = -[N]\,(G+D)$$

Similarly equation (1.7) can be written in matrix form as

1.17) $$\dot{\sigma} = [Z]\,(G+D)$$

The thermodynamic equation (1.10) is differenced consistent with the method employed in the hydrostatic equation. The potential temperature is written in terms of temperature and the last term becomes

$$\dot{\sigma}\frac{\partial\theta}{\partial\sigma} = - \frac{1}{2(\Delta\sigma_k)}\left[\dot{\sigma}_{k+1}\left(T_{k+1}\left(\frac{\hat{\sigma}_k}{\hat{\sigma}_{k+1}}\right)^{R/C_p} - T_k\right) + \dot{\sigma}_k\left(T_k - T_{k-1}\left(\frac{\hat{\sigma}_k}{\hat{\sigma}_{k-1}}\right)^{R/C_p}\right)\right] + \frac{RT_k}{C_p}\left(G_k - \bar{G} - \bar{D}\right).$$

For the purposes of the semi-implicit formulation described later in the paper, we separate the temperature into its horizontal average, T^*, and perturbation, T'. The matrix, [Y], is defined such that

$$\frac{T^*_{k+1}\left(\frac{\hat{\sigma}_k}{\hat{\sigma}_{k+1}}\right)^{R/C_p} - T^*_k}{2(\Delta\sigma_k)}\,\dot{\sigma}_k + \frac{T^*_k - \left(\frac{\hat{\sigma}_k}{\hat{\sigma}_{k-1}}\right)^{R/C_p} T^*_{k-1}}{2(\Delta\sigma_k)}\,\dot{\sigma}_k = [Y]\dot{\sigma}\ .$$

NAVAL

The vertically averaged divergence can be written $\bar{D} = [N]D$, so that

$$-[Y]\dot{\sigma} - \frac{RT^*}{C_p}\bar{D} = -[Y]\vec{\dot{\sigma}} - \frac{RT^*}{C_p}[N]D \; .$$

Substituting for $\dot{\sigma}$ from equation (1.17) we obtain

$$-[Y]\dot{\sigma} - \frac{RT_k^*}{C_p}[N]D = -[Y][Z]G - ([Y][Z] + \frac{RT^*}{C_p}[N])D$$

$$= -[S]G + [Q]D \; .$$

Finally the entire term can be written as

$$1.18) \quad \dot{\sigma}\frac{\partial\theta}{\partial\sigma} = -[S]G+[Q]D - \frac{1}{2(\Delta\sigma_k)}[\dot{\sigma}_{k+1}(T'_{k+1}(\frac{\hat{\sigma}_k}{\hat{\sigma}_{k+1}})^{R/C_p} - T'_k) + \dot{\sigma}_k(T'_k - (\frac{\hat{\sigma}_k}{\hat{\sigma}_{k-1}})^{R/C_p} T'_{k-1})] + \frac{RT_k}{C_p}(G_k - \bar{G}) - \frac{RT'_k}{C_p}\bar{D}$$

The nonlinear terms are computed using the transform method suggested by Orszag (1971). The longitudinal direction is done using Fast Fourier Transform and the latitudinal direction is done with Gaussian Quadrature. The number of latitudes, N, and longitudes, M, satisfy:

$$N \geq (3J+1)/2 \quad \text{and} \quad M \geq 3J+1 \; .$$

The number of points are picked to ensure non-aliased results for quadratic terms. Certain terms containing $\dot{\sigma}$ have triple products and are not computed alias free. Experiments by the author and a previous study (Hoskins and Simmons, 1975) indicate that this source of error is negligible for the length of the integrations performed in this study.

III. SEMI-IMPLICIT SCHEME

This section gives details of the semi-implicit time differencing scheme used in some of the experiments of this study. Using the matrices defined in the model description section, equations (1.9)-(1.12) can be written

2.1) $\frac{\partial D}{\partial t} + \nabla^2(\phi' + RT^* q) = F_D$

2.2) $\frac{\partial T}{\partial t} - [Q]D = F_T$

2.3) $\frac{\partial q}{\partial t} + [N]D = -\bar{G}$

2.4) $\phi' = [C]T$

where $\phi' = \phi - \phi_{sfc}$.

F_D and F_T represent the remaining terms in each equation which are not explicitly separated out. Following Robert et al. (1972), all the terms on the left hand side of equations (2.1)-(2.4) are time averaged. We define the following averaging operator and represent the local tendencies by a Leapfrog finite difference scheme:

$$\overline{(\quad)}^t = \frac{(\quad)^{t+\Delta t} + (\quad)^{t-\Delta t}}{2}$$

$$\frac{\partial}{\partial t}(\quad) \approx \delta_t(\quad) = \frac{(\quad)^{t+\Delta t} - (\quad)^{t-\Delta t}}{2(\Delta t)}$$

Equations (2.1)-(2.4) can then be written as

2.5) $\delta_t D = F_D - \nabla^2(\overline{\phi'}^t + RT^* \overline{q}^t)$

2.6) $\delta_t T = F_T + [Q]\,\overline{D}^t$

2.7) $\delta_t q = - \bar{G} - [N]\,\overline{D}^t$

2.8) $\overline{\phi'}^t = [C]\,\overline{T}^t$

Eliminating $\overline{\phi'}^t$ in equation (2.5) by substitution of Eq. (2.8), we arrive at a time averaged set of equations:

2.9) $\overline{D}^t = D^{t-\Delta t} + (\Delta t)(F_D - \nabla^2([C]\overline{T}^t + RT^* \overline{q}^t))$

2.10) $\overline{T}^t = T^{t-\Delta t} + (\Delta t)(F_T + [Q]\,\overline{D}^t)$

2.11) $\overline{q}^t = q^{t-\Delta t} - (\Delta t)(\bar{G} + [N]\,\overline{D}^t)$.

Substituting equations (2.11) and (2.10) into (2.9) and solving for $\overline{D}^t$ we obtain a Helmholtz equation for the time averaged divergence

2.12) $([I]+(\Delta t)^2[B]\nabla^2)\overline{D}^t = D^{t-\Delta t} + (\Delta t)[F_D - \nabla^2([C]T^{t-\Delta t}$

$+(\Delta t)[C]F_T + RT^* q^{t-\Delta t} - (\Delta t)\, RT^* \bar{G}]$

where [I] is the identify matrix and $[B] = [C][Q] - RT^*[N]$.

For a spectral formulation, the equation is trivial to solve since the spherical harmonics are eigenfunctions of the Laplacian ∇^2. Knowing $\overline{D}^t$, we then compute the prognostic

NAVAL

variables $T^{t+\Delta t}$, $q^{t+\Delta t}$ from equations (2.6) - (2.7). $D^{t+\Delta t}$ is computed from the definition of the time averaging operator:

$$D^{t+\Delta t} = 2\overline{D}^{t} - D^{t-\Delta t}$$

and the vorticity, $\zeta^{t+\Delta t}$, never entered the semi-implicit formalism and is computed from a standard Leapfrog scheme. Calculations with the semi-implicit model required 5% more computer time per time step. Stable integrations were possible with a time step of 60 mins.

IV. QUASI-GEOSTROPHIC DIVERGENCE

Following the analysis of Simmons and Hoskins (1976), a diagnostic divergence is obtained for the case of quasi-geostrophic flow with the full variation of the Coriolis parameter over the sphere. The relevant equations become

$$3.1)\quad \frac{\partial\zeta}{\partial t} = - V_{\psi} \cdot \nabla(\zeta+f) - \mathcal{L}D$$

$$3.2)\quad \mathcal{L}\zeta - \nabla^{2}(\phi' + RT^{*}q) = 0$$

$$3.3)\quad \frac{\partial T}{\partial t} = - V_{\psi} \cdot \nabla T + \hat{\dot{\sigma}} \left(\frac{R}{C_{p}} \frac{T^{*}}{\sigma} - \frac{\partial T^{*}}{\partial\sigma}\right)$$

where V_{ψ} - rotational part of V

$\hat{\dot{\sigma}}$ - sigma dot at odd levels

$\mathcal{L}D = \nabla \cdot (f\nabla(\nabla^{-2}D))$

Making use of the hydrostatic relationship, equation (1.15), we may write equation (3.3) as

$$\frac{\partial\phi'}{\partial t} = -[C](V_{\psi} \cdot \nabla T) + \gamma^{*} \hat{\dot{\sigma}}$$

where $\gamma^{*} = [C] \left(\frac{R}{C_{p}} \frac{T^{*}}{\sigma} - \frac{\partial T^{*}}{\partial\sigma}\right).$

Taking ∇^{2} of this equation, $\mathcal{L}$ of equation (3.1) and $\frac{\partial}{\partial t}$ of eq. (3.2) and substituting we arrive at the following equation for $\hat{\dot{\sigma}}$:

$$3.4)\quad \gamma^{*}\hat{\dot{\sigma}} = -\nabla^{-2}[(V_{\psi}\cdot\nabla(\zeta+f))+ \quad {}^{2}D]+[C](V_{\psi}\cdot\nabla T)+RT^{*}\nabla^{2} \frac{\partial q}{\partial t} .$$

NAVAL

A second equation for $\dot{\sigma}$ is obtained from the continuity equation in the form of eq. (1.17), which when explicitly written out, is

$$3.5)\quad \dot{\sigma} = \sigma(\bar{D} + \bar{G}) - \int_{0}^{\sigma} (D + G)\, d\sigma$$

where $\dot{\sigma}$ is specified on even levels.

The diagnostic $\hat{\dot{\sigma}}$ from equation (3.4) can be used to compute the divergence using eq. (3.5) provided we specify a boundary condition. For the purposes of initialization, this is most conveniently chosen to be

$$\frac{\partial q}{\partial t} = -\,(\bar{D} + \bar{G}) \equiv 0$$

since this will tend to eliminate external gravity waves. Applying this constraint to equations (3.4) and (3.5) we obtain

$$3.6)\quad \gamma^{*}\hat{\dot{\sigma}} = -\nabla^{-2}(\,(V_{\psi}\cdot\nabla(\zeta+f)) + \mathcal{L}^{2}D) + [C]V_{\psi}\cdot\nabla T$$

$$3.7)\quad \hat{\dot{\sigma}} = -\int_{0}^{\sigma} (D + G)\, d\sigma\,.$$

The method of solution will be to compute $\hat{\dot{\sigma}}$ using equation (3.6) from an initial guess of the divergence. The even level $\dot{\sigma}$'s are then found by interpolation and a new guess of the divergence is obtained by inverting equation (3.7). The updated divergence can be substituted back into equation (3.6) and the procedure continues iteratively until sufficient accuracy is obtained.

Equations (3.6) and (3.7) will now be put into spectral form. The equations contain three similar advective terms. It will be sufficient to show the spectral form of one of them:

$$3.8)\quad V_\psi \cdot \nabla(\zeta+f) = -J(\psi, \zeta+f) = -\frac{1}{r^2}\left(\frac{\partial\psi}{\partial\mu}\frac{\partial\zeta}{\partial\lambda} - \frac{\partial\psi}{\partial\lambda}\frac{\partial(\zeta+f)}{\partial\mu}\right) .$$

First, the terms are individually transformed to physical space by the summations:

$$\frac{\partial\psi}{\partial\mu} = \sum_{\ell,m} \psi_\ell^m \frac{\partial P_\ell^m}{\partial\mu} \ell^{im\lambda}$$

$$\frac{\partial\zeta}{\partial\lambda} = \sum_{\ell,m} im\, \zeta_\ell^m P_\ell^m \ell^{im\lambda}$$

$$\frac{\partial\psi}{\partial\lambda} = \sum_{\ell,m} im\, \psi_\ell^m P_\ell^m \ell^{im\lambda}$$

$$\frac{\partial(\zeta+f)}{\partial\mu} = \sum_{\ell,m} \xi_\ell^m \frac{\partial P_\ell^m}{\partial\mu} \ell^{im\lambda} + 2\Omega .$$

The multiplications in eq. (3.8) are then computed at grid points and the result is transformed back to spectral space by computing the inner product defined as:

$$3.9)\quad J_L^M = \frac{1}{4\pi}\int_{-1}^{+1}\int_{0}^{2\pi} J(\psi, \zeta+f) Y_L^M \, d\lambda d\mu \equiv \langle J(\psi, \zeta+f),\ Y_L^M\rangle .$$

The integral is computed using Gaussian quadrature in the μ direction and Fast Fourier Transforms in the λ direction. The first term of equation (3.6) can then be evaluated:

$$\begin{aligned}\mathcal{L}(V_\psi \cdot \nabla(\zeta+f)) &= \nabla \cdot (f\nabla(\nabla^2 J)) \\ &= fJ + \frac{2\Omega(1-\mu^2)}{r^2}\frac{\partial}{\partial\mu}(\nabla^2 J)\end{aligned}$$

and expanded in spectral form using the previous computation of J_ℓ^m:

$$< (V\psi \cdot \nabla(\zeta+f))\, Y_L^M > = \Omega \int_{-1}^{+1} \mu(\sum_\ell J_\ell^M P_\ell^M) P_L^M d\mu - \Omega \int_{-1}^{+1} (1-\mu^2)(\sum_\ell \frac{J_\ell^M}{\ell(\ell+1)} \frac{\partial P_\ell^M}{\partial \mu}) P_L^M \, d\mu \ ,$$

where the λ integration has already been done.

Making use of the recurrence relationship

$$\mu P_\ell^M = \varepsilon_{\ell+1}^M \, P_{\ell+1}^M + \varepsilon_\ell^M \, P_{\ell-1}^M$$

$$\varepsilon_\ell{}^M = \sqrt{\frac{\ell^2 - M^2}{4\ell^2 - 1}} \quad ,$$

we can write the first integrand as

$$\sum_\ell \mu \, J_\ell^M \, P_\ell^M = \sum_\ell J_{\ell-1}^M \, \varepsilon_\ell^M \, P_\ell^M + \sum_\ell J_{\ell+1}^M \, \varepsilon_{\ell+1}^M \, P_\ell^M$$

and using the orthogonality of the Legendre polynomials we obtain for the first integral

$$3.10) \quad \int_{-1}^{+1} \mu(\sum_\ell J_\ell^M P_\ell^M) P_L^M \, d\mu = J_{L-1}^M \, \varepsilon_L^M + J_{L+1}^M \, \varepsilon_{L+1}^M \ .$$

The second integral can be done similarly using the relationship

$$(1-\mu^2)\frac{\partial P_\ell^M}{\partial \mu} = (\ell+1) \, \varepsilon_\ell^M \, P_{\ell-1}^M - \ell \varepsilon_{\ell+1}^M \, P_{\ell+1}^M$$

to obtain

$$3.11)\int_{-1}^{+1}(1-\mu^2)(\sum_{\ell}\frac{J_{\ell}^M}{\ell(\ell+1)}\frac{\partial P_{\ell}^M}{\partial\mu}P_L^M\,d\mu = J_{L+1}^M\frac{\varepsilon_{L+1}^M}{L+1} - J_{L-1}^M\frac{\varepsilon_L^M}{L} .$$

Combining eqs (3.10) and (3.11) we obtain

$$3.12)\quad <\mathfrak{L}(V_{\psi}\cdot\nabla(\zeta+f),Y_L^M> = \Omega[\frac{L+1}{L}\varepsilon_L^M J_{L-1}^M + \frac{L}{L+1}\varepsilon_{L+1}^M J_{L+1}^M] .$$

The second order operator $\mathfrak{L}^2D$ can now be formulated. Using the notation, $<\mathfrak{L}D,\ Y_L^M> = F_L^M$, we can write by analogy with equation (3.12)

$$F_L^M = \Omega[\frac{L+1}{L}\varepsilon_L^M D_{L-1}^M + \frac{L}{L+1}\varepsilon_{L+1}^M J_{L+1}^M] .$$

Thus,

$$\mathfrak{L}D = \sum_{\ell,m} F_{\ell}^M Y_{\ell}^M$$

and

$$<\mathfrak{L}^2D,\ Y_L^M> = <\mathfrak{L}(\mathfrak{L}D),\ Y_L^M> = \Omega[\frac{L+1}{L}\varepsilon_L^M F_{L-1}^M + \frac{L}{L+1}\varepsilon_{L+1}^M F_{L+1}^M] .$$

Substituting in for F_{L-1}^M and F_{L+1}^M, we obtain the result

$$\begin{aligned}3.13)\quad <\mathfrak{L}^2D,Y_L^M> = \Omega^2[(&\frac{(L+1)L}{L(L-1)}\varepsilon_L^M\varepsilon_{L-1}^M)D_{L-2}^M \\ &+ (\frac{L^2-1}{L^2}(\varepsilon_L^M)^2 + \frac{L^2+2L}{(L+1)^2}(\varepsilon_{L+1}^M)^2)D_L^M \\ &+ (\frac{L^2+L}{(L+1(L+2)}\varepsilon_{L+1}^M\ \varepsilon_{L+2}^M)\ D_{L+2}^M] .\end{aligned}$$

NAVAL

Finally, eqs (3.6) and (3.7) may now be fully expanded as

$$3.14)\quad \hat{\dot{\sigma}}_L^M = \frac{1}{\gamma^*}\left[R_L^M + \frac{r^2}{\ell(\ell+1)}\left(\langle \mathcal{L}(V_\psi \cdot \nabla\zeta + f), Y_L^M\rangle + \langle \mathcal{L}^2 D, Y_L^M\rangle\right)\right]$$

$$3.15)\quad \dot{\sigma}_L^M = -\int_0^\sigma (D_L^M + G_L^M)\, d\sigma$$

where

$$R_L^M = [C]\ \langle V_\psi \cdot \nabla T,\ Y_L^M\rangle\ .$$

V. DESIGN OF THE EXPERIMENTS

The initial conditions used in the experiments of this thesis were developed from a baroclinically unstable mean flow and a small perturbation in zonal wave no. 6 (m=6). The mass field of the mean flow was constrained to be in geostrophic thermal balance with the mean wind. The vertical profile of the mean wind was linear varying from 4.5 m/sec at $\sigma = 1$ to 49.5 m/sec at $\sigma = 0$. The latitudinal structure varied as $\sin^2(2\eta)$ placing a jet max at $\eta = 45°$. The vertical temperature profile approximated the U. S. Standard Atmosphere.

The perturbation in wave no. 6 corresponded to a maximum v-component of .1 m/sec. The model was integrated for 192 hrs allowing the baroclinic wave to grow to finite amplitude. Fig. 2 shows a time series of the vorticity during this period. The growth is strikingly linear until 192 hrs where there is evidence of the mean flow (m = 0) changing due to feedback from the eddies. The linear growth corresponds to a doubling time of roughly 26 hrs for m = 6. The fields at 192 hrs provided the balanced fields for the initialization experiments.

Three types of experiments and one control case were integrated for 72 hrs of model time.

NAVAL

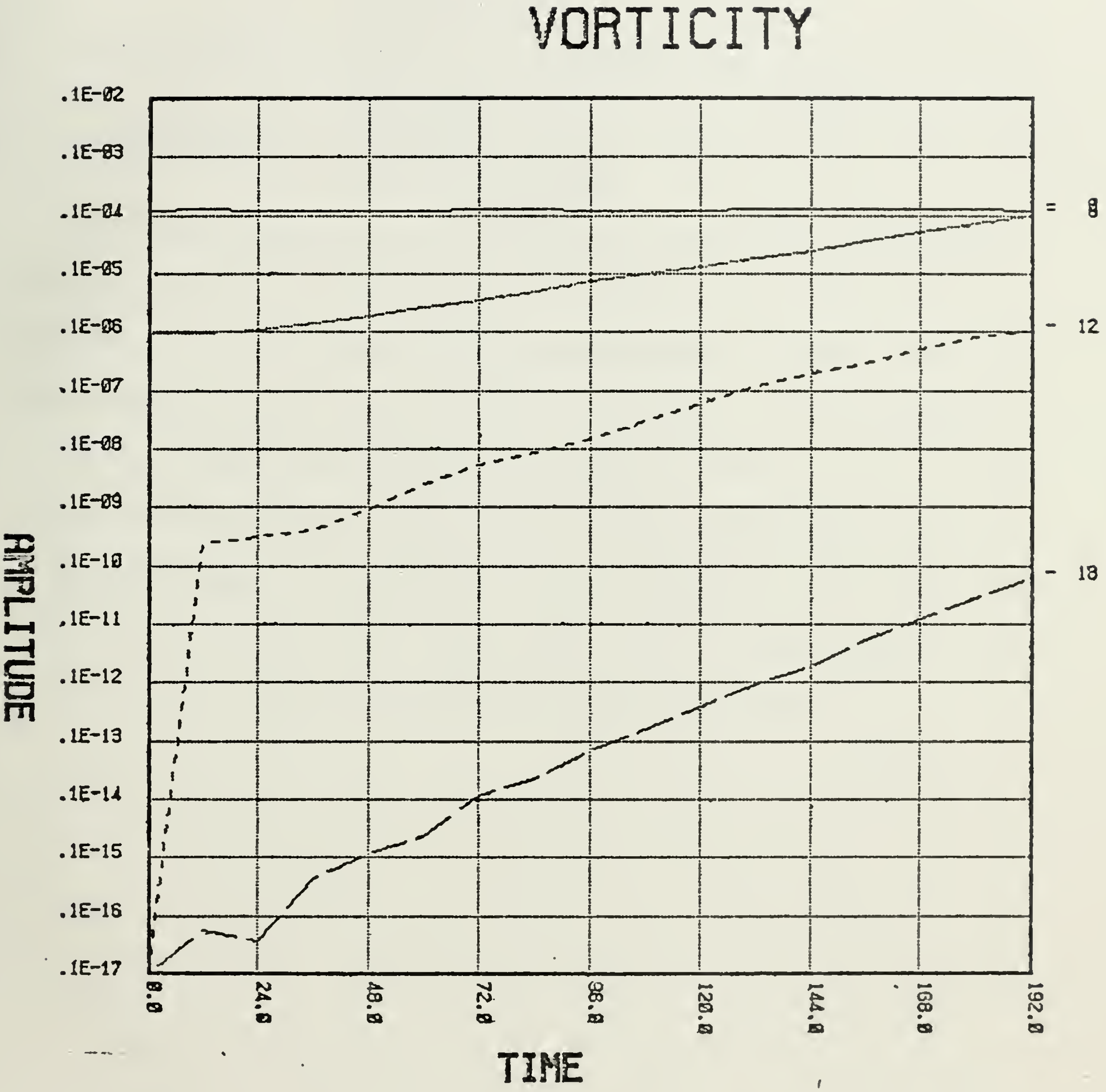

Figure 2. Vorticity time series during the first 192 hrs. Vertical axis is logarithmic. Units are secs^{-1}. Solid curve is the magnitude of wave no. 0 at latitude 60°N. Dotted curve is m=6, short dashes are m=2 and long dashes are m=18.

The control case consisted of initializing with the balanced fields and integrating. The experiments consisted of the following:

Experiment A: Initialize with the balanced fields but no divergence

Experiment B: Initialize with the balanced fields plus the quasi-geostrophic divergence

Experiment C: Identical to Experiment A but with a semi-implicit scheme

All experiments and the control were first integrated with a spectral truncation of wave no. 21. These will be referred to as low resolution experiments. High resolution experiments were integrated for the control and Experiments A and B. These cases were truncated at wave no. 42. Time steps of 12 mins for the low resolution and 6 mins for the high were used. Experiment C was integrated with time steps of 12 and 60 mins. All experiments had a weak Robert time filter of 0.1 and no dissipation term was used.

VI. RESULTS

A. CONTROL CASE

Figures 3-6 show the initial fields at level 5 for the low resolution experiments. Figures 7-10 are the corresponding high resolution fields. They are characterized by a developing frontal zone. The advantage of the high resolution is apparent in the temperature gradients across the cold front and warm front and in the surface pressure. The low in the high resolution surface pressure field is 5 mb deeper. The negative and positive areas of the divergence and vorticity fields are approximately symmetrical in the low resolution fields and quite asymmetric in the high resolution fields. The region of maximum positive vorticity corresponds very well with the maximum temperature gradient.

The mean fields consist of an indirect cell induced by the growing baroclinic eddies. The indirect cell develops in order to decrease the vertical wind shear which must remain in approximate thermal balance with the decreasing pole to equator temperature gradient. The effect is more pronounced in the low resolution fields. The high resolution mean fields contain a weak indirect circulation and a strong direct cell.

The dynamic situation during the period of the control case is one of a rapid cascade of energy to smaller scales.

NAVAL

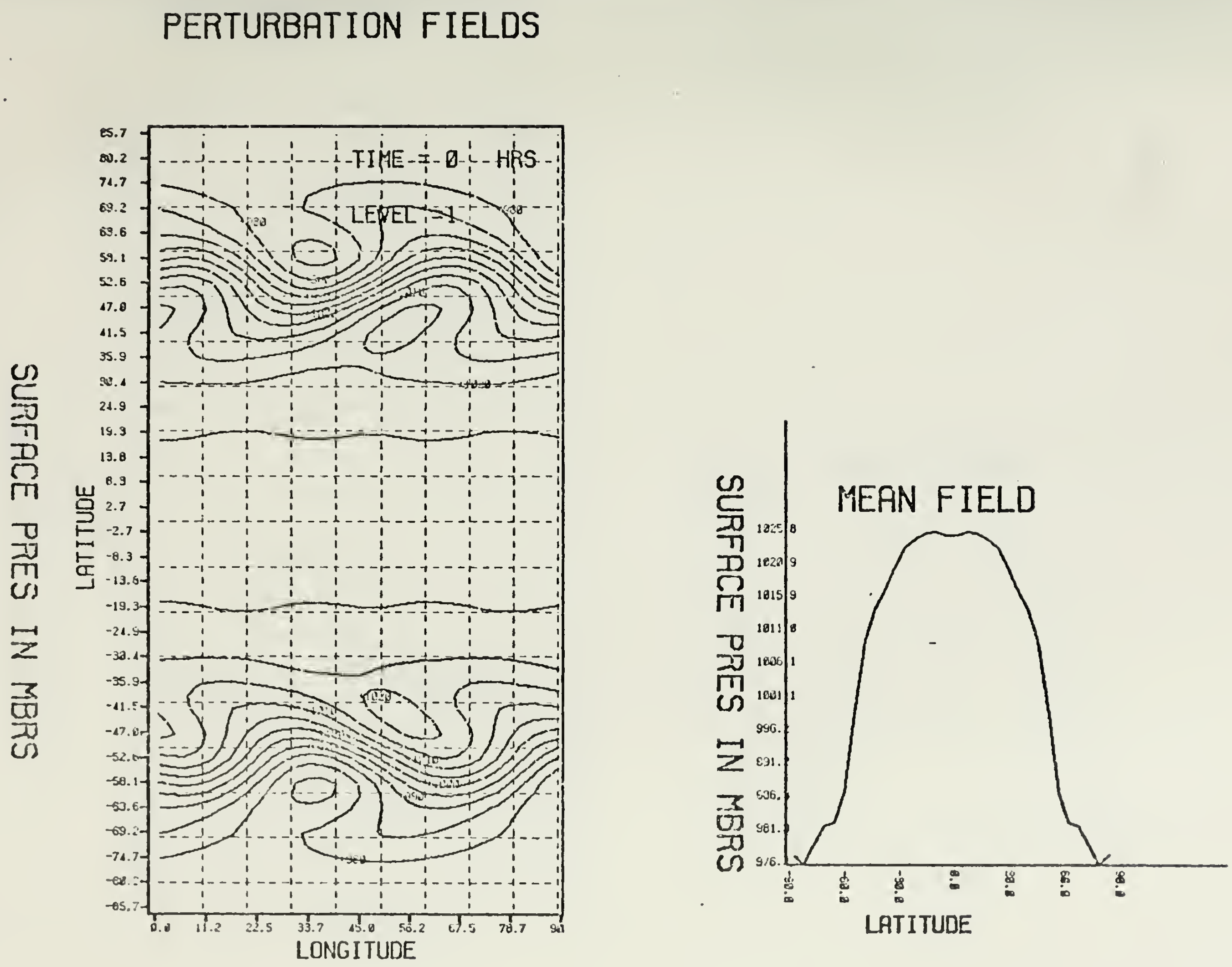

Figure 3. Initial low resolution surface pressure. Contour interval is 5 mb.

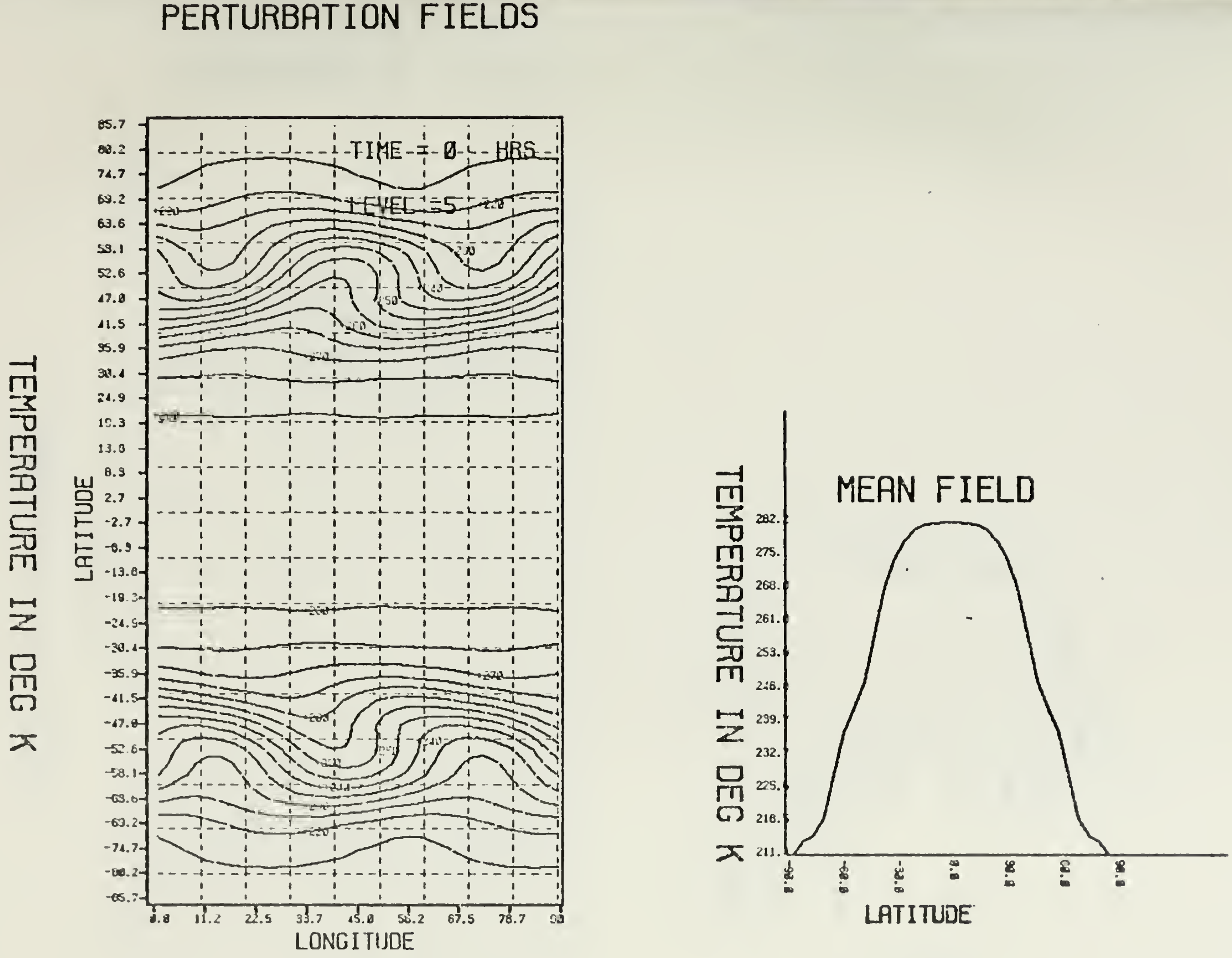
PERTURBATION FIELDS

MEAN FIELD

Figure 4. Initial low resolution temperature for σ = .9. Contour interval is 5°K.

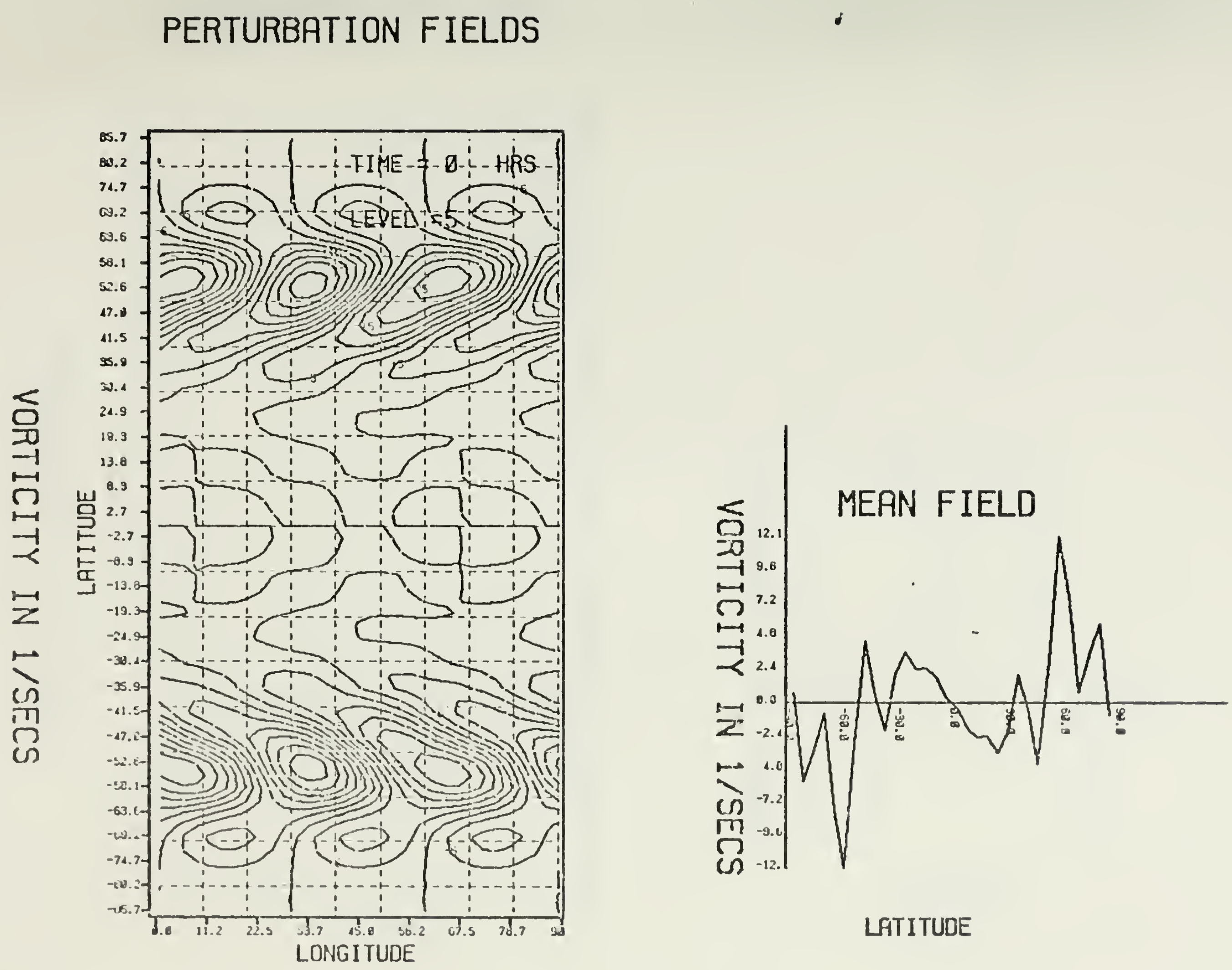

Figure 5. Initial low resolution vorticity for $\sigma = .9$. Contour interval is $5\times10^{-6}\text{sec}^{-1}$. Mean field is scaled by 10^6.

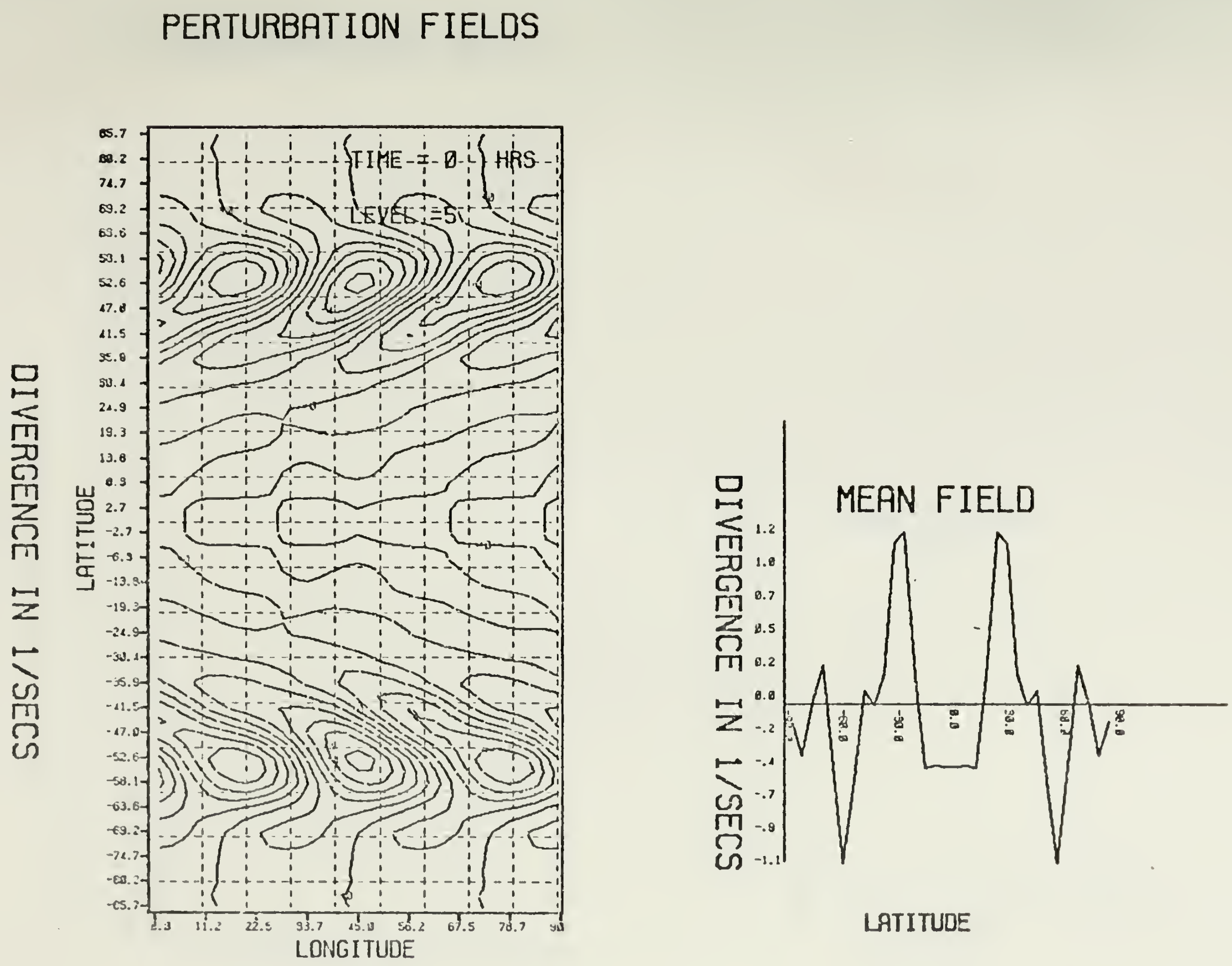

Figure 6. Initial low resolution divergence for $\sigma = .9$. Contour interval is $1 \times 10^{-6} \mathrm{sec}^{-1}$. Mean field is scaled by 10^6.

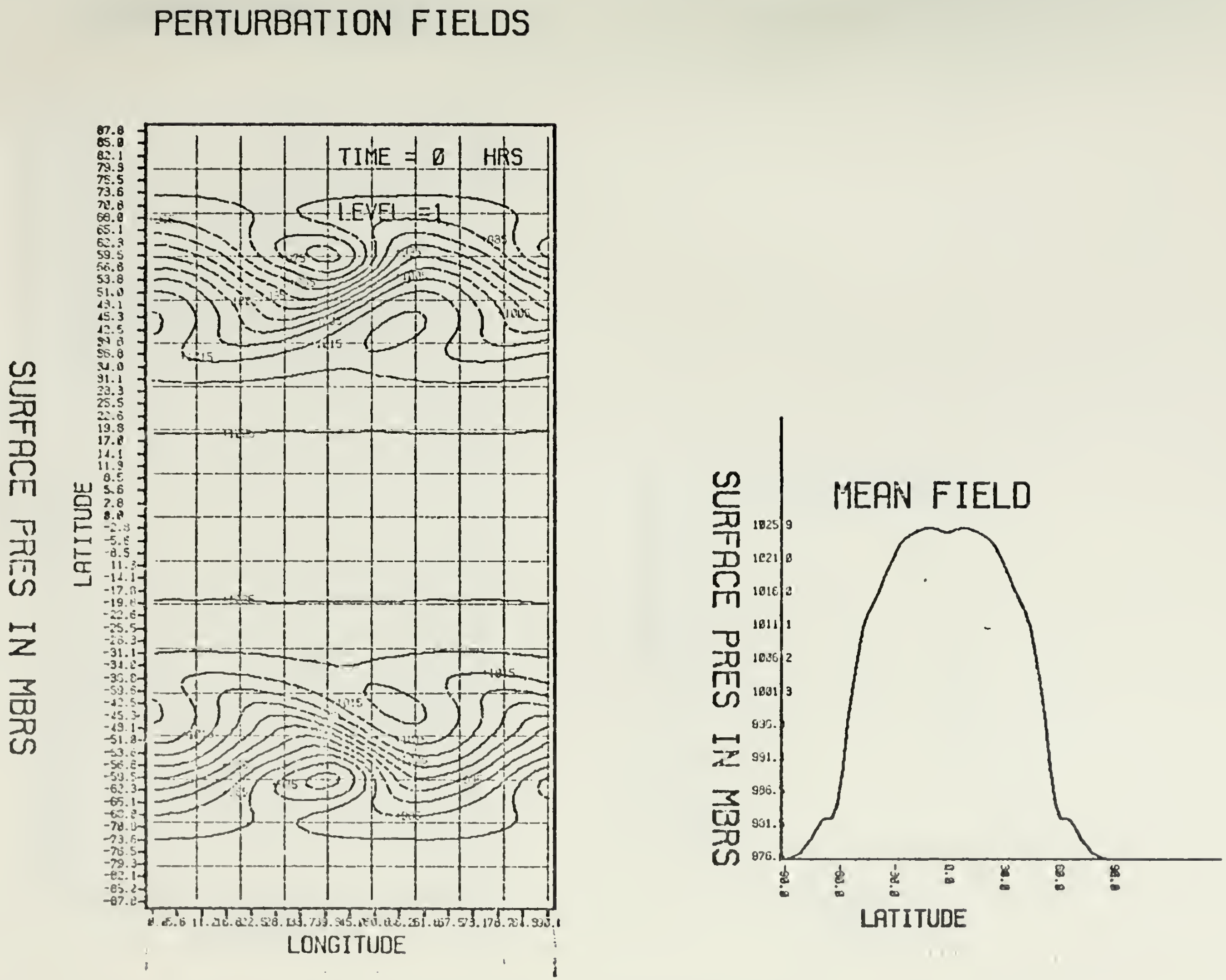

Figure 7. Initial high resolution surface pressure. Contour interval is 5 mb.

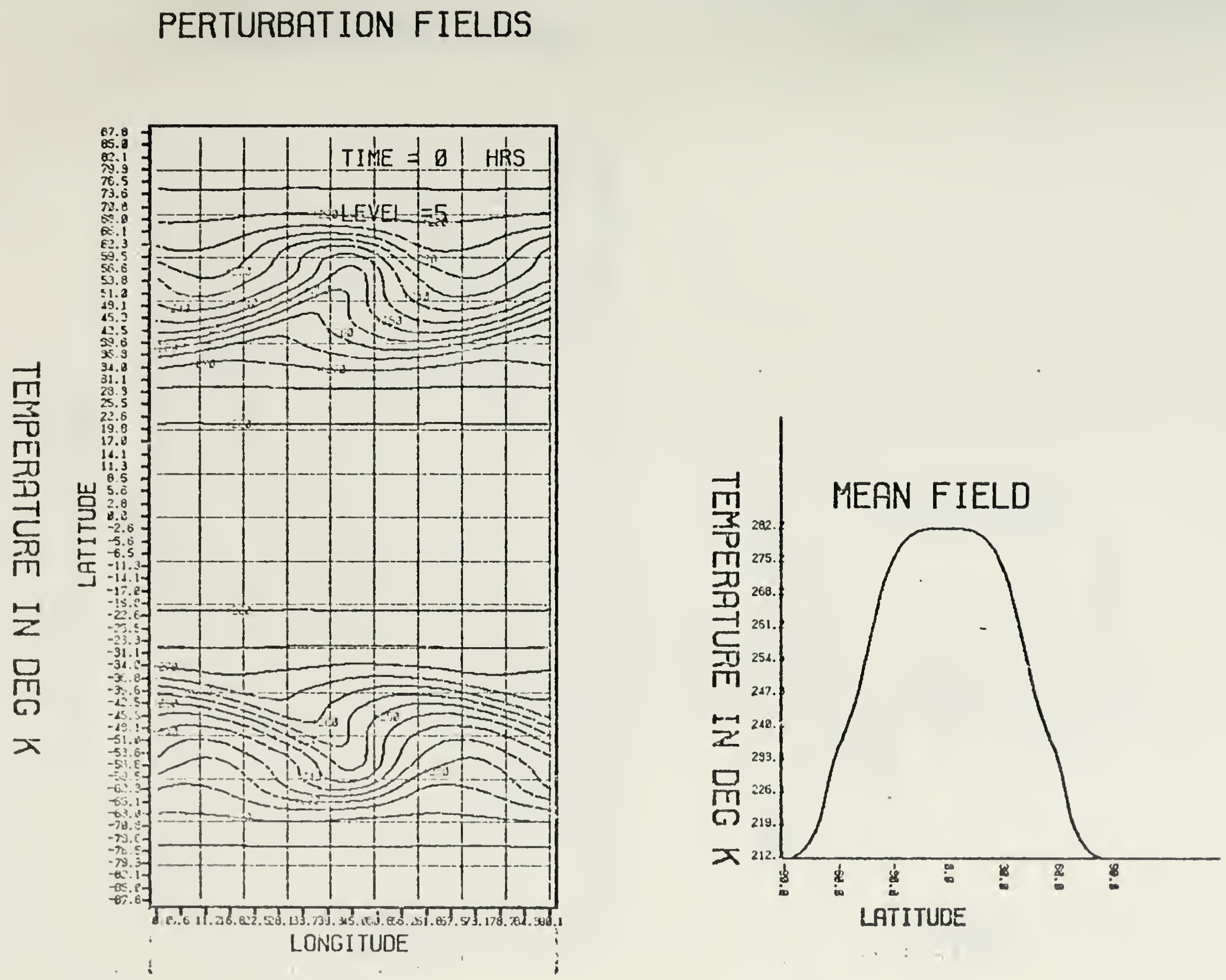

Figure 8. Initial high resolution temperature for σ = .9. Contour interval is 5°K.

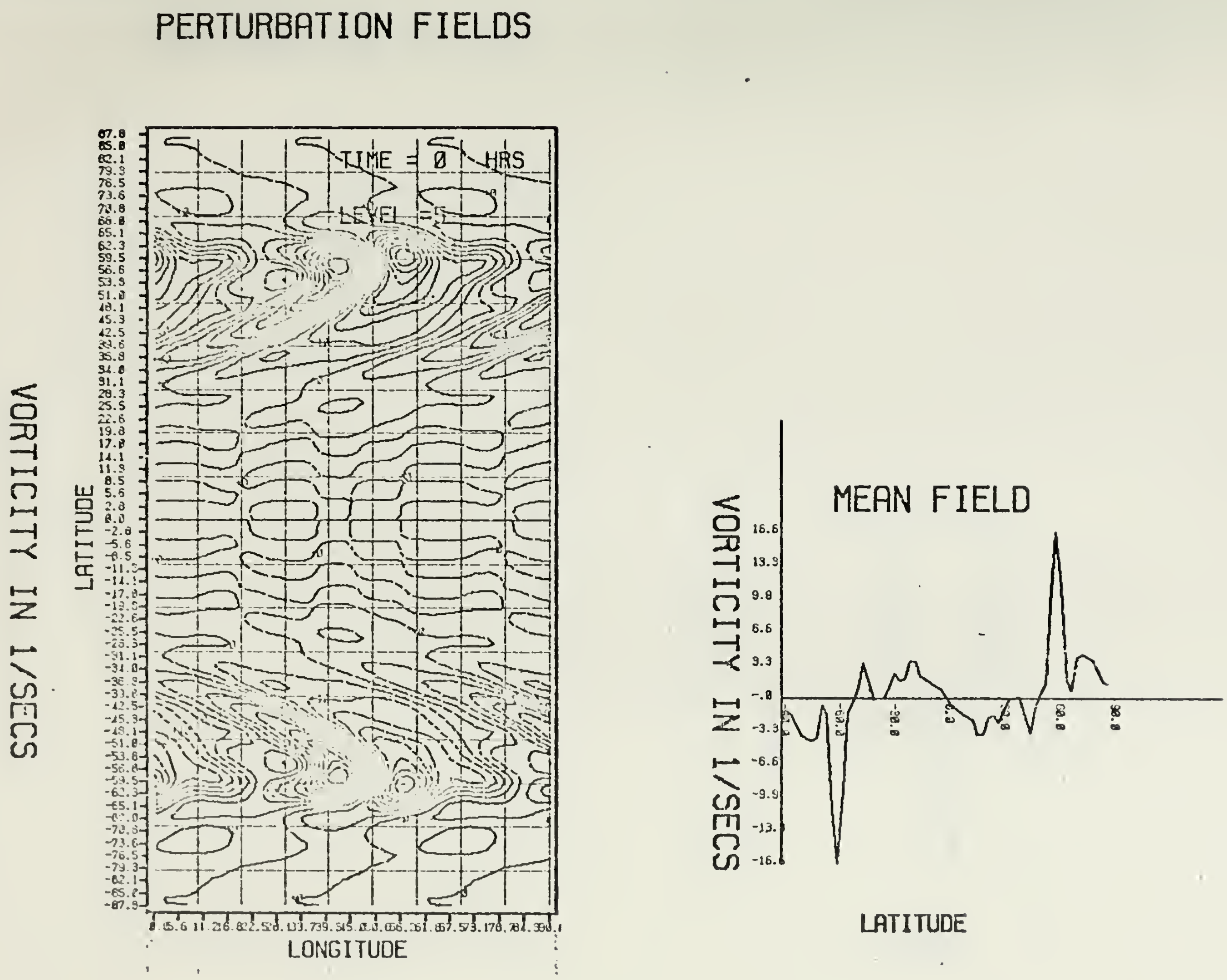

Figure 9. Initial high resolution vorticity for σ = .9. Contour interval is $5 \times 10^{-6} sec^{-1}$. Mean field is scaled by 10^6.

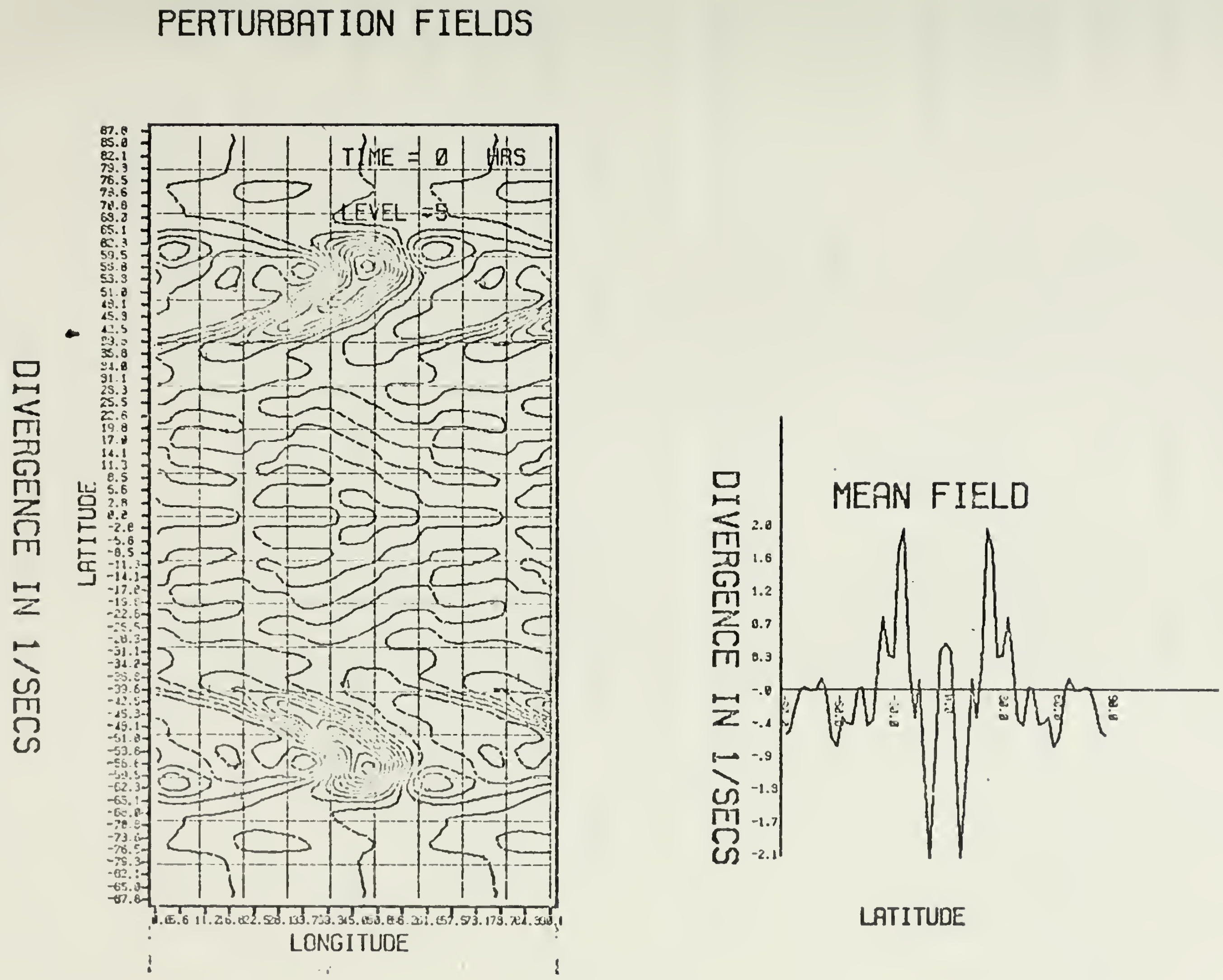

Figure 10. Initial high resolution divergence for $\sigma = .9$. Contour interval is $1 \times 10^{-6} sec^{-1}$. Mean field is scaled by 10^6.

the horizontal scale of the frontal zone decreases. Figures 11-13 show this effect in the high resolution temperature fields for times out to 36 hr. Beyond this point, the energy builds up at the spectral limit of the model since there is no dissipation and the 72 hr fields are non-meteorological (Fig. 14 and 15). Because the energy blockage occurs at smaller scales, the high resolution case (Fig. 14) is, paradoxically, noisier and in greater error.

B. GRAVITY WAVES

In anticipation of later sections, we discuss the characteristics of inertial gravity waves for the model used in this study. The divergence is the most sensitive indicator of gravity wave motion. As discussed in Hoskins and Simmons (1975), equation (2.12) is the semi-implicit analogue of the gravity wave equation for a multi-layer model. The eigenvalues of the matrix [B] (eq. 2.12) give the permissible eigenvelocities of the gravity wave modes. The corresponding eigenvectors give the vertical structure. Figure 16 depicts the eigenmodes for the experiments in this study. Table I gives the periods of the gravity wave modes for zonal wave no. 6 in hrs.

TABLE I

External	First	Second	Third	Fourth
3.31	11.1	28.0	61.7	154

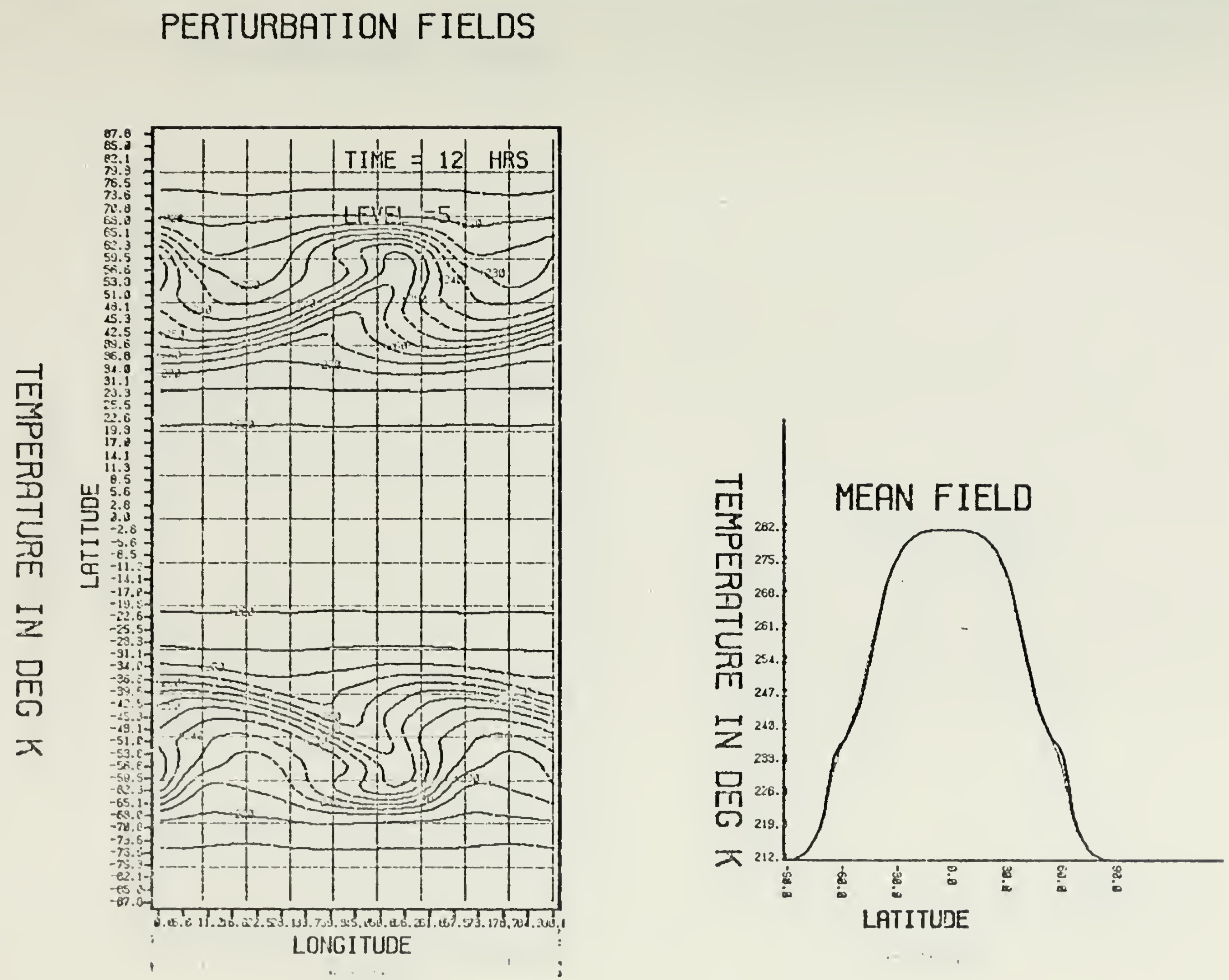

Figure 11. 12 hr high resolution temperature for σ = .9. Contour interval is 5°K.

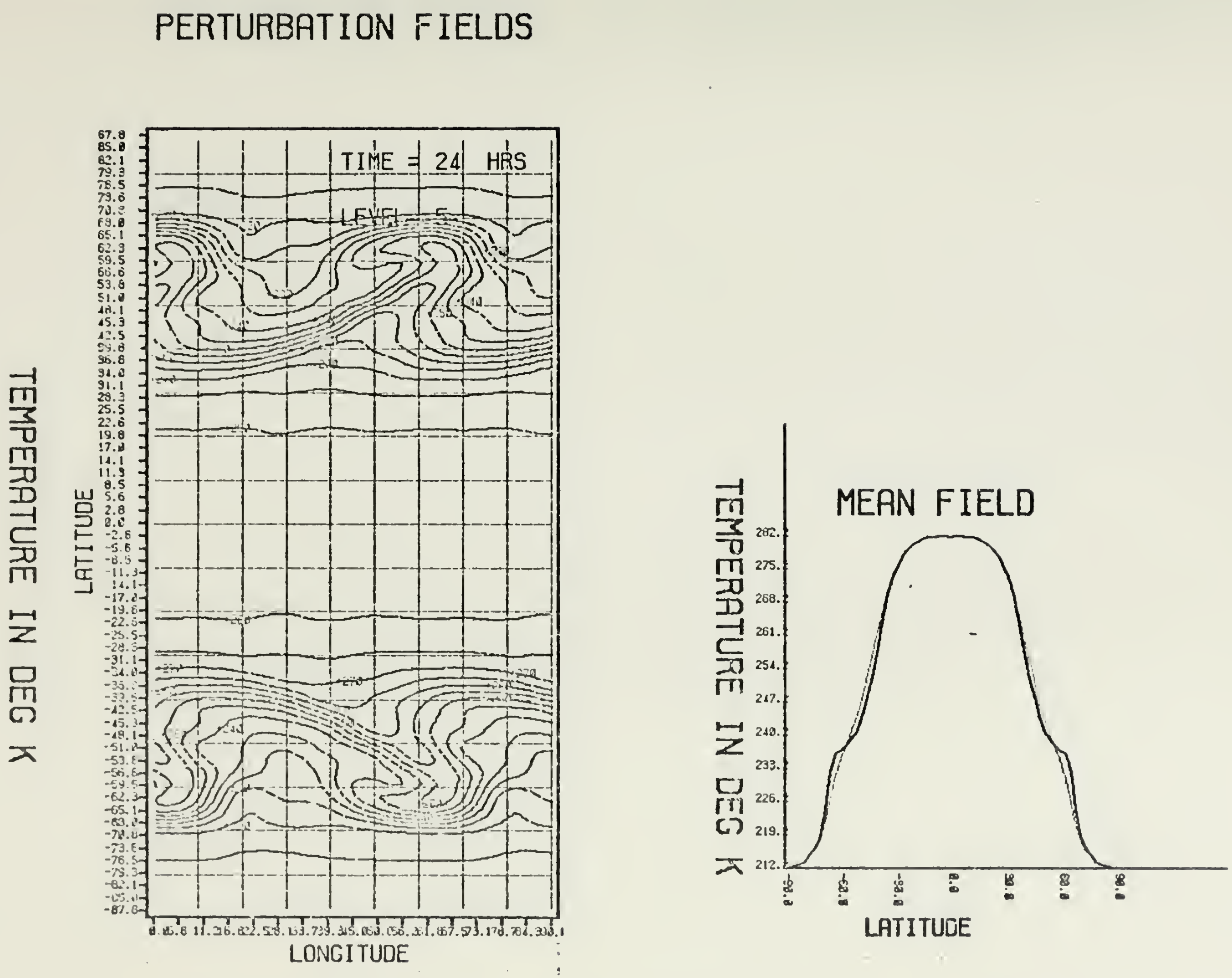

Figure 12. 24 hr high resolution temperature for $\sigma = .9$. Contour interval is 5°K.

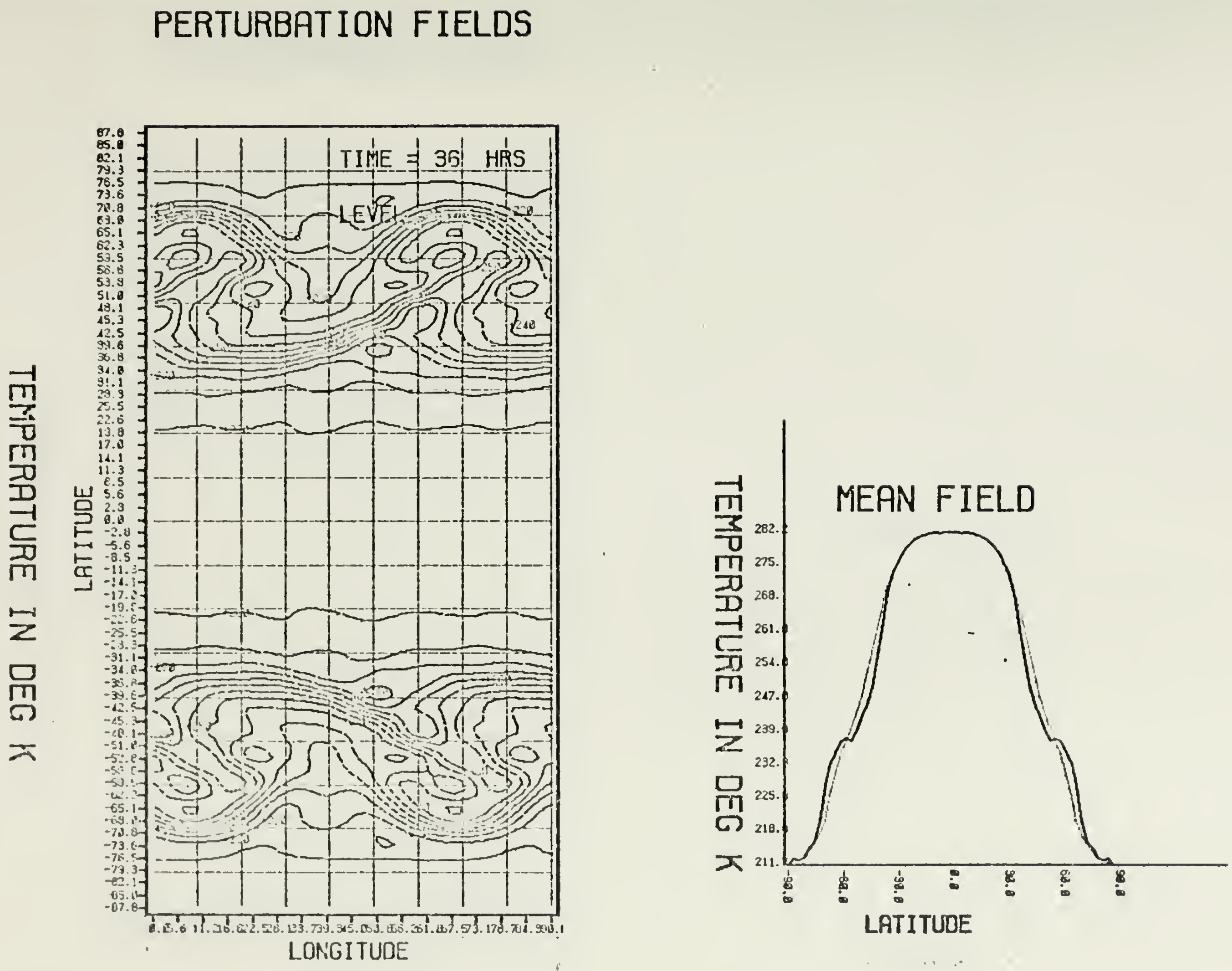

Figure 13. 36 hr high resolution temperature for $\sigma = .9$. Contour interval is 5°K.

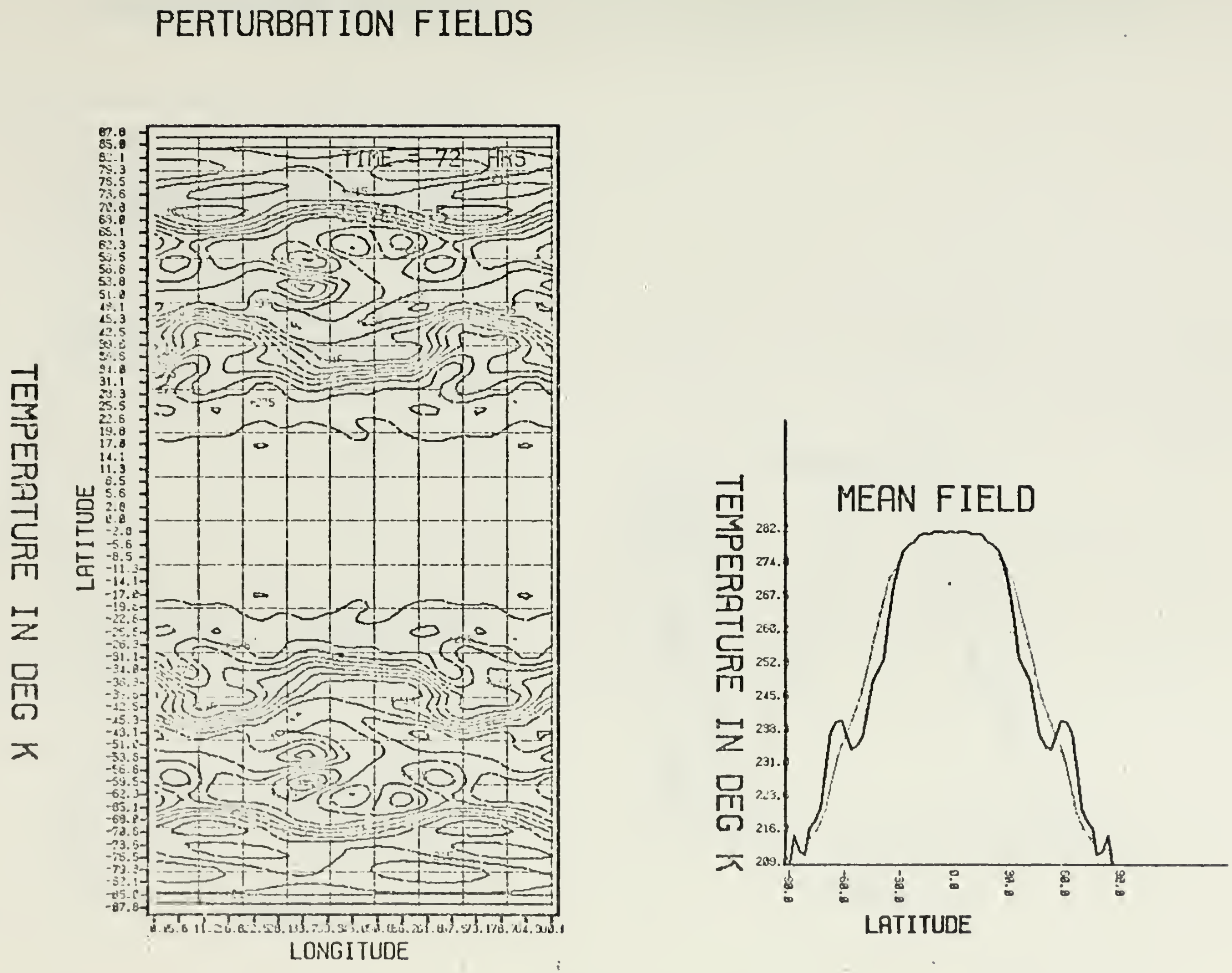

Figure 14. 72 hr high resolution temperature for $\sigma = .9$. Contour interval is 5°K.

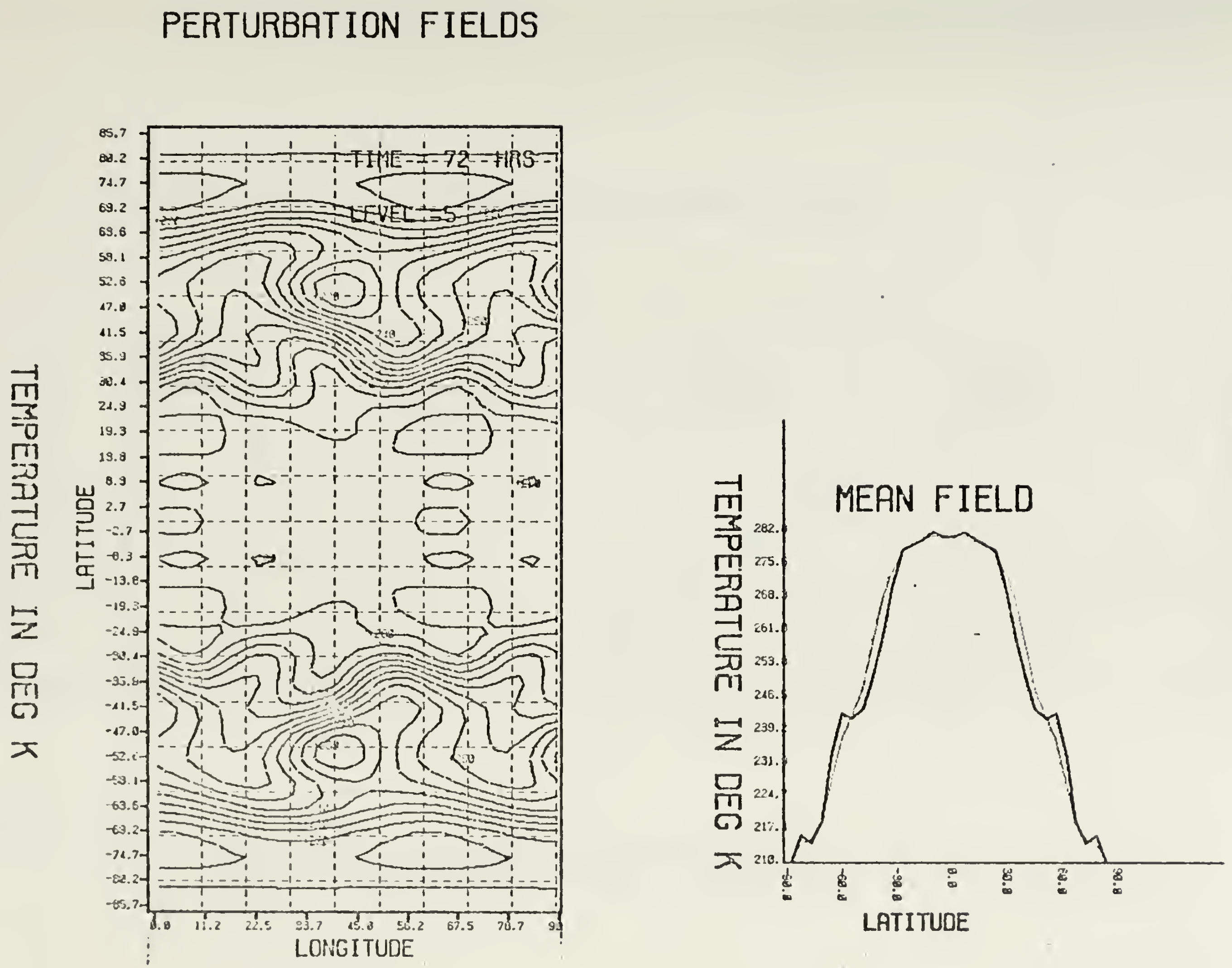

Figure 15. 72 hr low resolution temperature for σ = .9. Contour interval is 5°K.

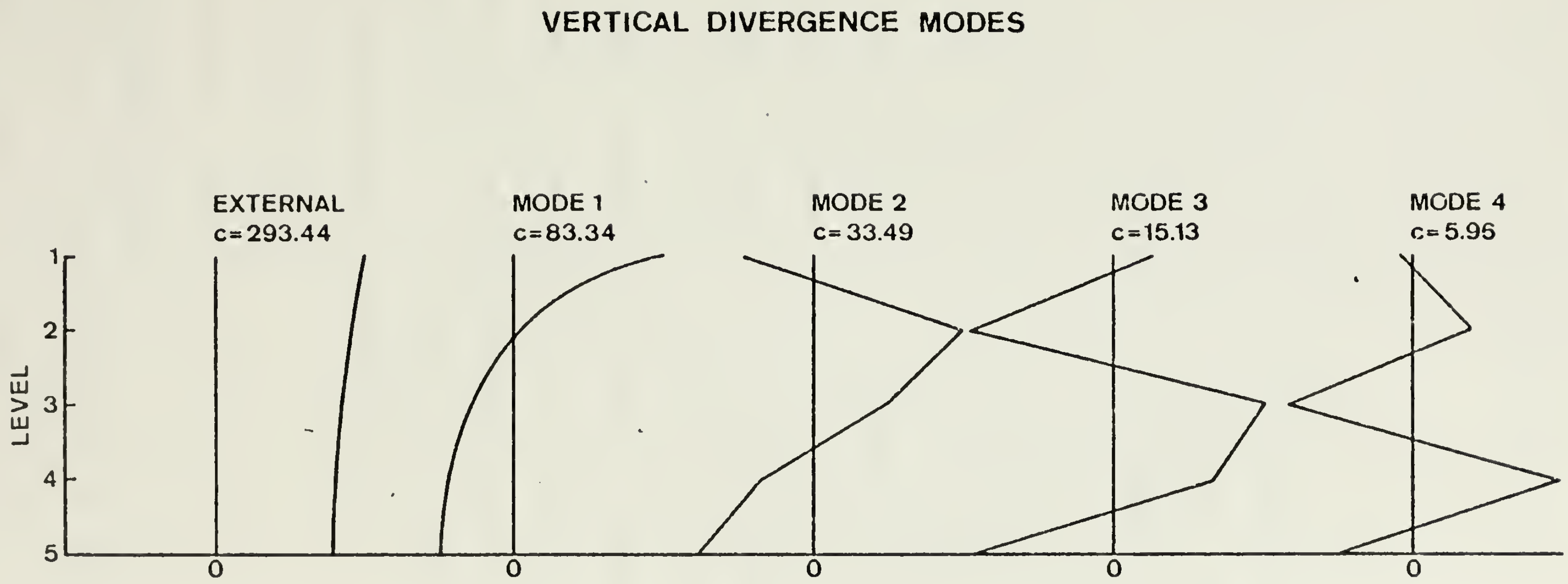

Figure 16. Structure and eigenvelocities of the external and four internal divergence modes. Velocities are in m/sec.

The total divergence may be thought of as consisting of a sum of the individual eigenmodes:

$$4.1)\qquad D = \sum_k a_k D_k$$

where the D_k are the eigenvectors. The weighting coefficients, a_k, may be obtained from the simultaneous equations formed by the dot products of the individual eigenvectors with equation (4.1). A time series of the coefficients will provide useful diagnostic information in later sections. Figures 17 and 18 are a time series of the external and first internal modes for the low resolution control case at a point on the 60° latitude circle. It is apparent that the coefficients contain both the meteorological modes and any excited gravity modes. Figure 17 contains no high frequency oscillation and is purely meteorological. Figure 18 contains a meteorological mode with a period of roughly 3 days plus a smaller amplitude wave whose period of approximately 1/2 day corresponds well with the calculated value for the first internal mode from Table 1. The remaining internal gravity modes have periods approaching meteorological values and are difficult to distinguish.

C. EXPERIMENTS A AND B

1. Low Resolution

Neglecting the divergence in the initialized fields (Experiment A) generated computational gravity waves. Comparing the pressure tendencies of the control case (Fig. 19c)

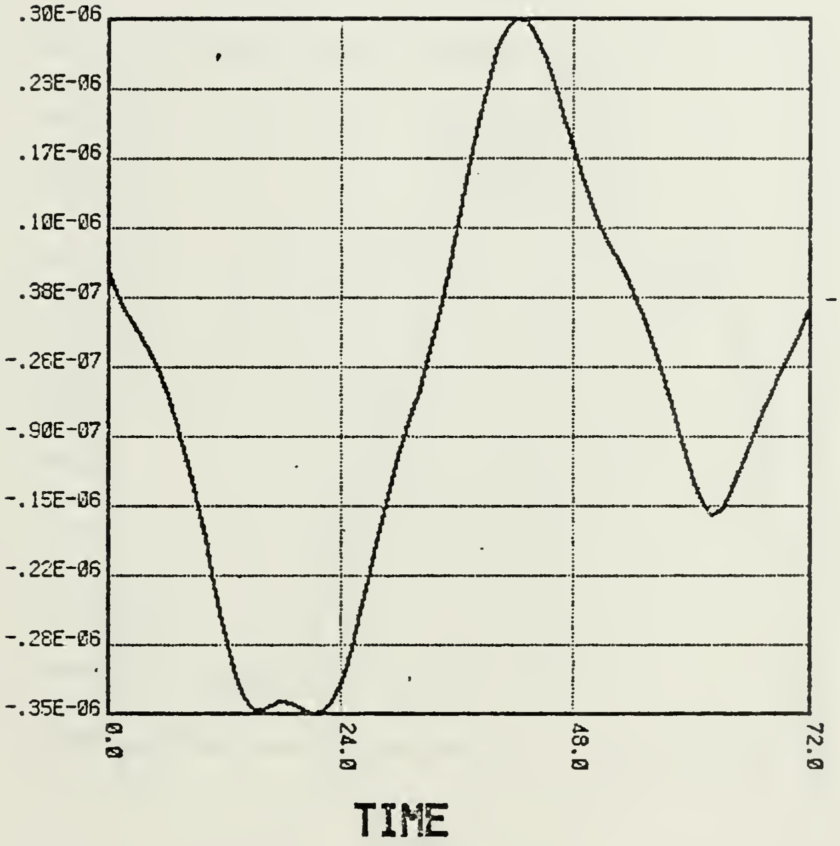

Figure 17. Divergence time series of the external mode for the low resolution control case. Vertical axis units are $\sec^{-1}$. Time is in hrs.

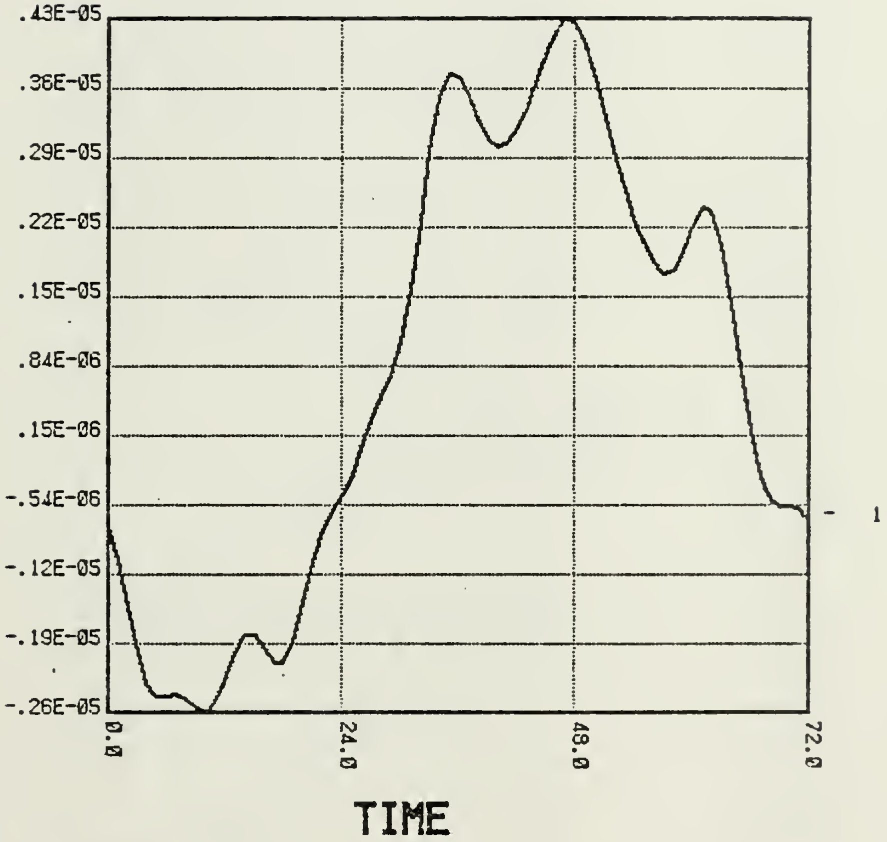

Figure 18. Time series of the first internal mode - otherwise as in Fig. 17.

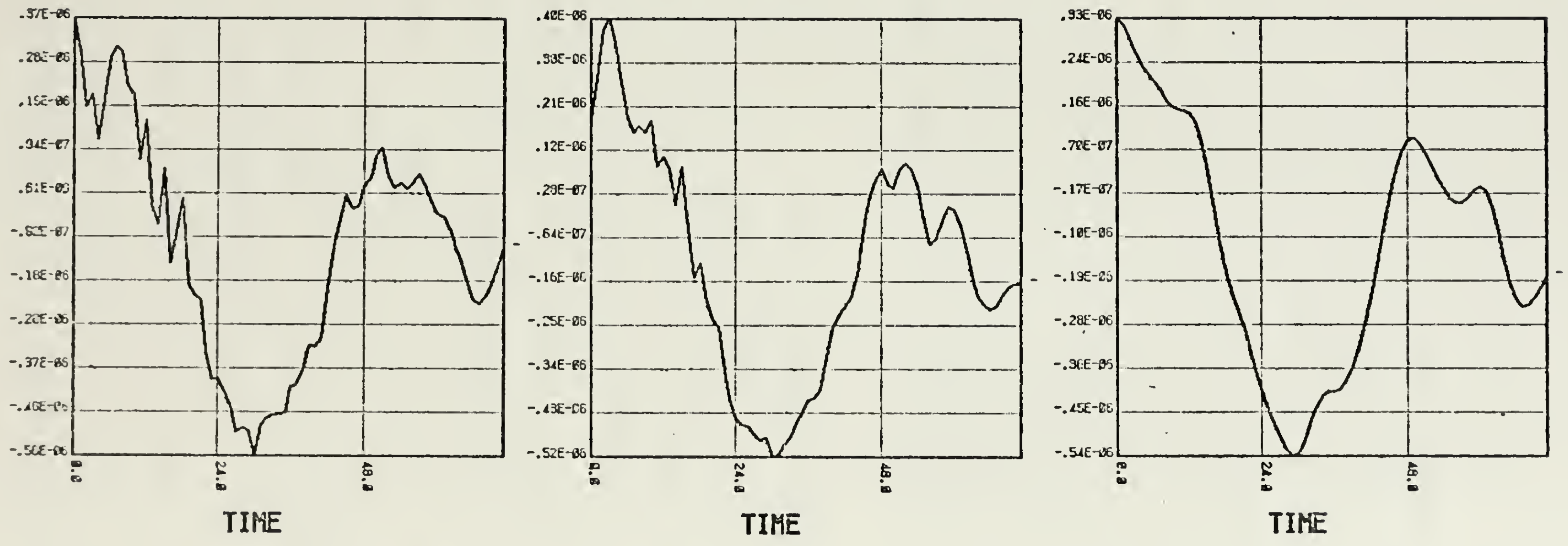

19a 19b 19c

Figure 19. $\partial q/\partial t$ for a low resolution Experiment A (19a), Experiment B (19b) and the control case (19c). Time is in hrs. Vertical scale is sec^{-1}.

with those of Experiment A in Fig. 19a, it is apparent that high frequency oscillations of roughly 3 hr period are excited. The initial magnitudes of the oscillations are approximately 1-2 mb/hr. The oscillations dampen out with time as the geostrophic adjustment takes place although the dispersal of the gravity waves during the adjustment process is hampered by the longitudinal periodicity and the symmetry of the fields about the equator.

Figure 19b shows the pressure tendencies with the quasi-geostrophic divergence inserted into the initialization fields (Experiment B). The highest frequency oscillations have been reduced over Experiment A by a factor of approximately 2.

Comparison of the divergence modes in Figs 20, 21, 22 allows us to be more quantitative. The figures have the control case subtracted out and contain the gravity wave noise generated by the approximations of each experiment. The noise generated in the internal modes by the non-divergent initialization is an order of magnitude larger than the external mode and is generally 25% of the total divergence. The figures show that the external mode of Experiment B is about 68% of Experiment A. The first internal mode shows more noise in Experiment B initially and then decreasing to 50% and the second internal mode shows a decrease of about 50% over Experiment A. In general the effect of the quasi-geostrophic divergence is to reduce the gravity wave noise.

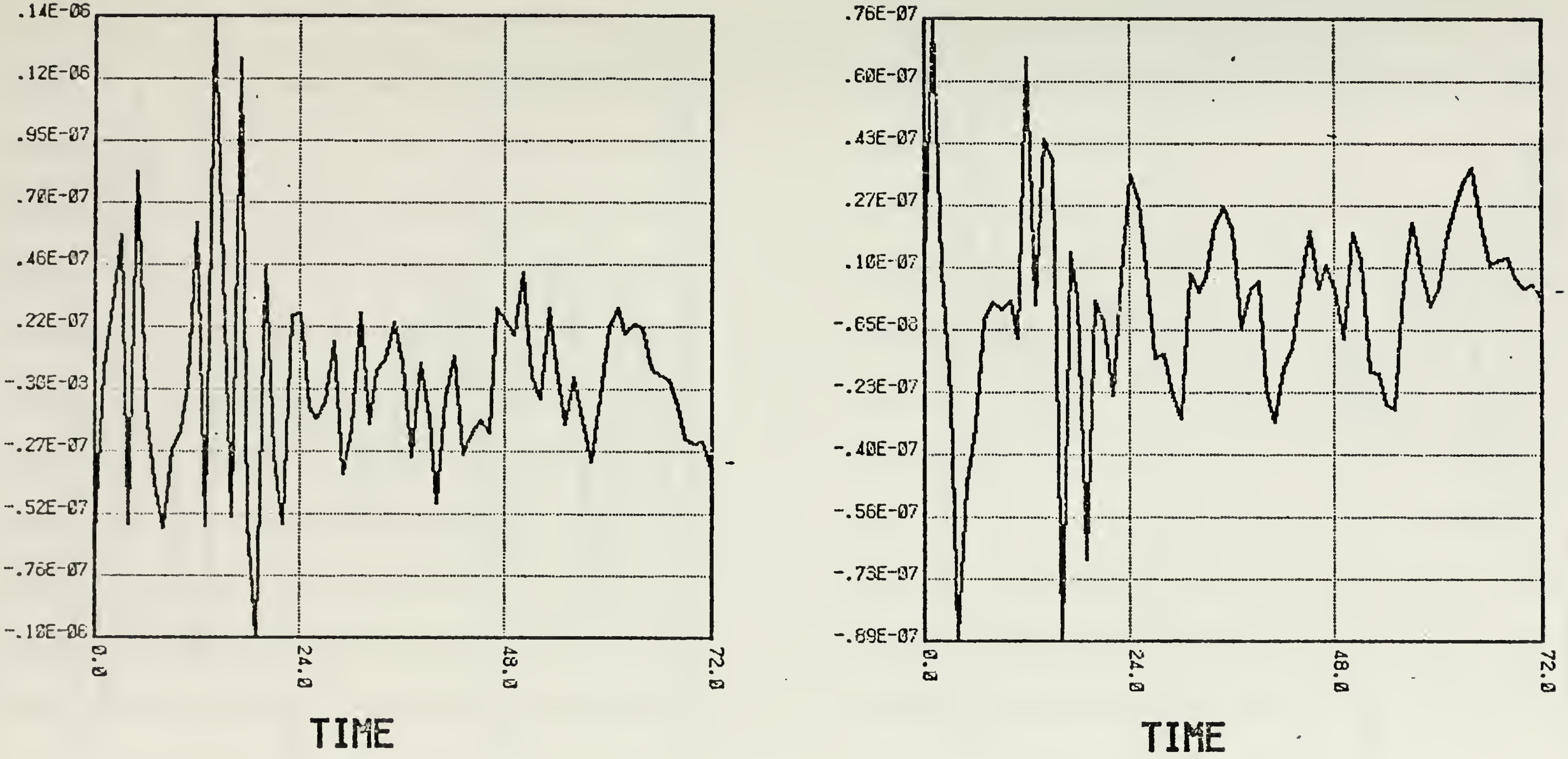

20a

20b

Figure 20. Gravity wave noise in the external mode for low resolution Experiment A (20a) and Experiment B (20b). Vertical scale is sec^{-1}. Time is in hrs.

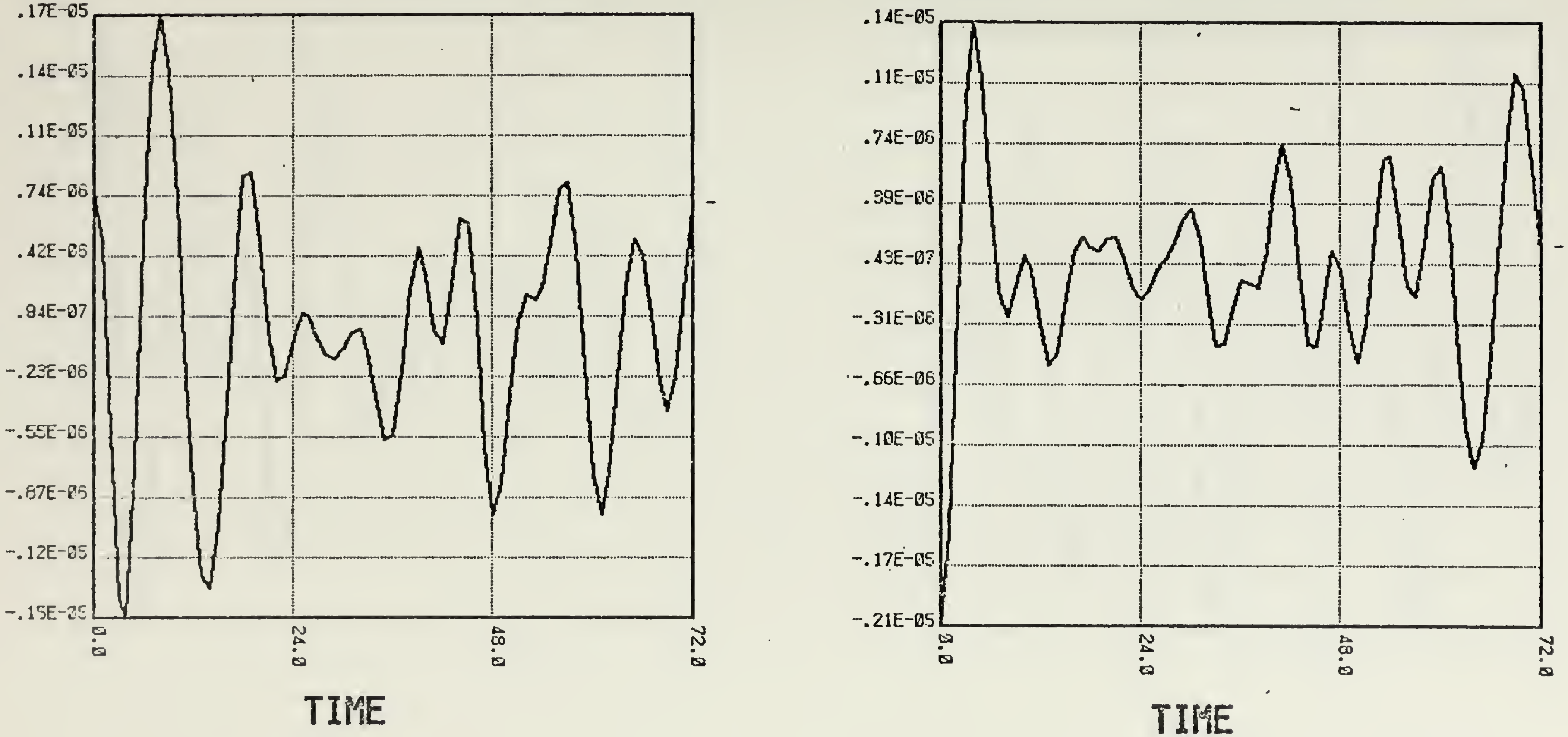

21a

21b

Figure 21. Gravity wave noise in the first internal mode - otherwise as in Fig. 20.

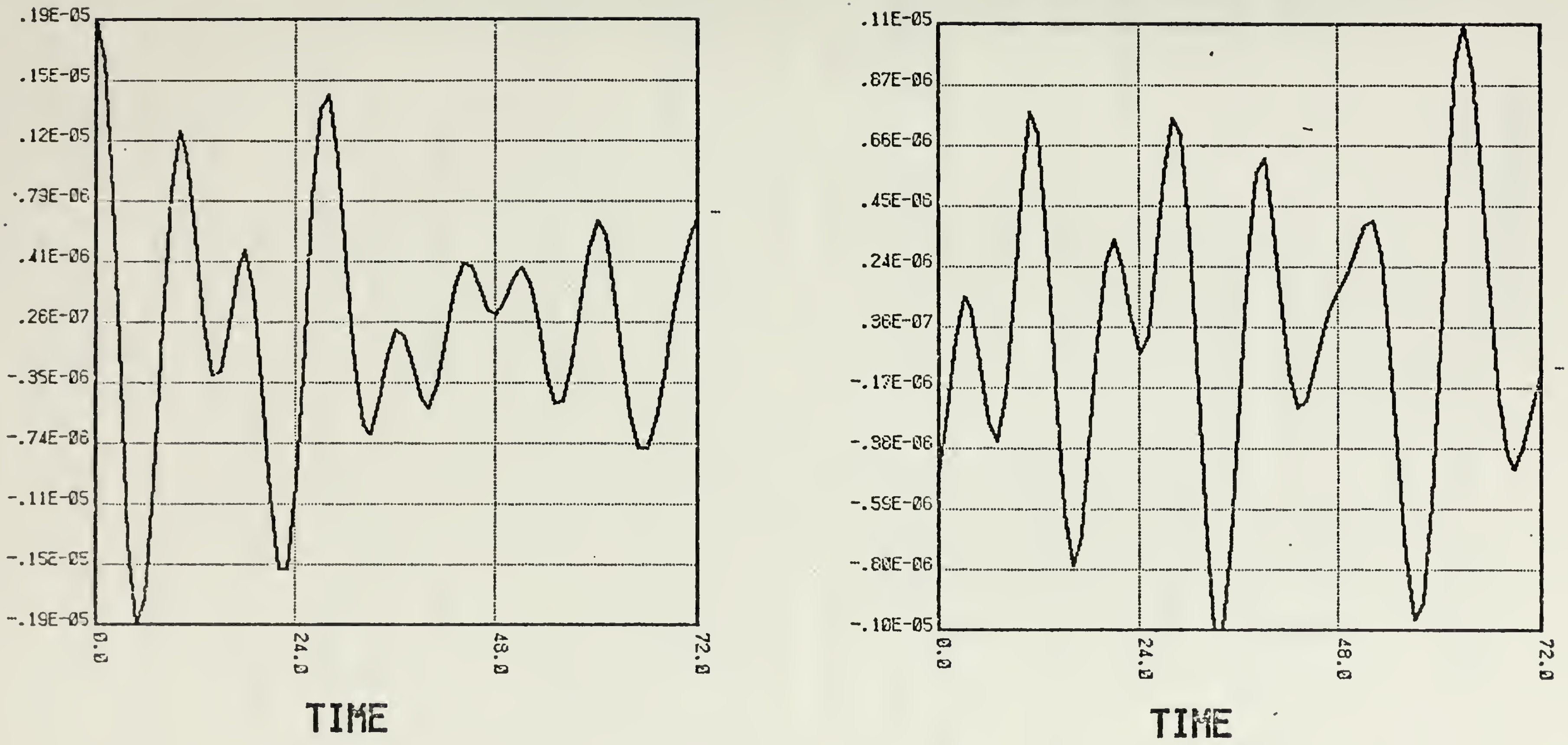

22a

22b

Figure 22. Gravity wave noise in the second internal mode - otherwise as in Fig. 20.

2. High Resolution

Figure 23 shows the quasi-geostrophic divergence at level 5 which was used for Experiment B. A qualitative comparison with the actual model divergence (Fig. 10) shows the phases to be in agreement but that the quasi-geostrophic approximation is an overestimate for the perturbation fields. The zonal mean fields do not compare well. The quasi-geostrophic divergence shows a strong indirect circulation which is displaced poleward relative to the model divergence. There is no evidence of a direct cell.

Figures 24-26 depict the noise generated in the divergence modes for Experiments A and B. Generally they show that the gravity wave noise of Experiment B is 66%-72% of that in Experiment A. The effect of the quasi-geostrophic divergence is to reduce the noise. However, this reduction is less than in the low resolution experiments.

In view of the fact that the high resolution experiments were less successful than the low resolution and that quasi-geostrophic formulations are valid only for small values of the Rossby number, it is interesting to compare the initial model divergence of the control case with the quasi-geostrophic divergence in a spectral manner. Referring to Fig. 27, it is seen that there is good agreement between the model and quasi-geostrophic divergences for zonal waves corresponding to $m = 6, 12, 18$. The overestimation by the quasi-geostrophic divergence noted earlier is primarily in wave no. 6. The mean fields ($m=0$) and waves corresponding to $m = 24,30,36,42$ do not compare well.

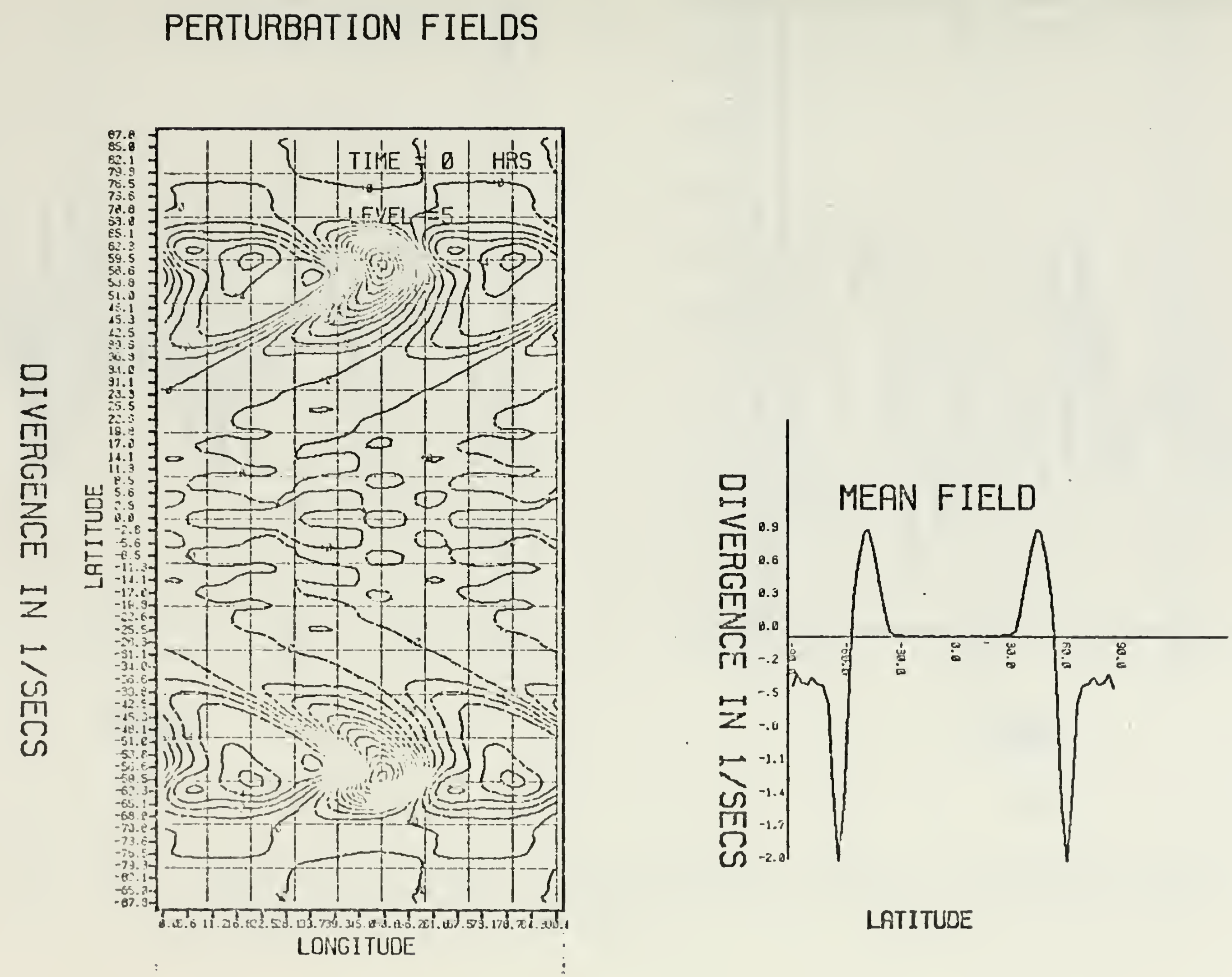

Figure 23. Quasi-geostrophic divergence (high resolution) for $\sigma = .9$. Contour Interval is $1 \times 10^{-6} sec^{-1}$. Mean field is scaled by 10^6.

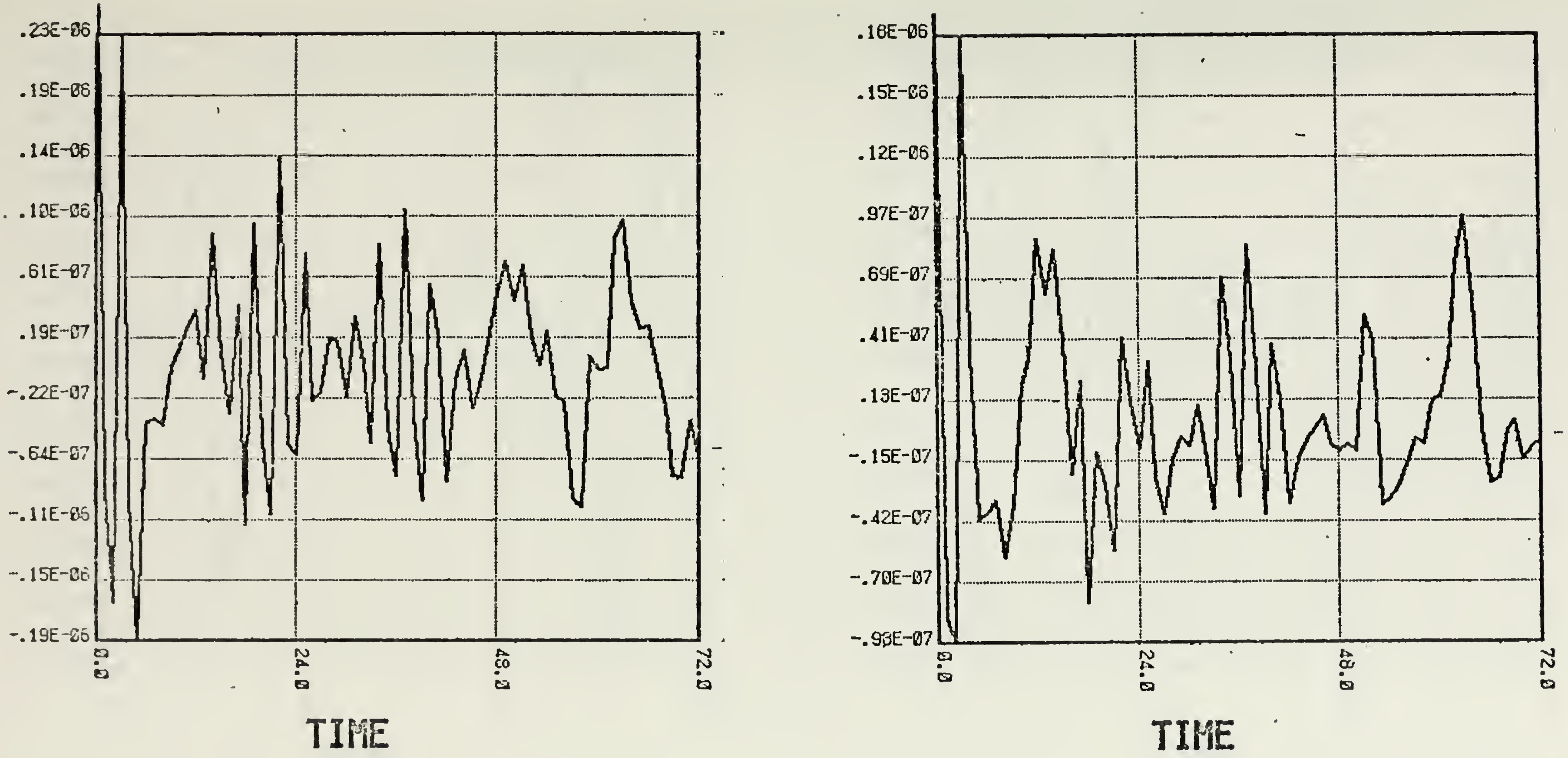

24a

24b

Figure 24. Gravity wave noise in the external mode for high resolution Experiment A (24a) and Experiment B (24b). Vertical scale is sec^{-1}. Time is in hrs.

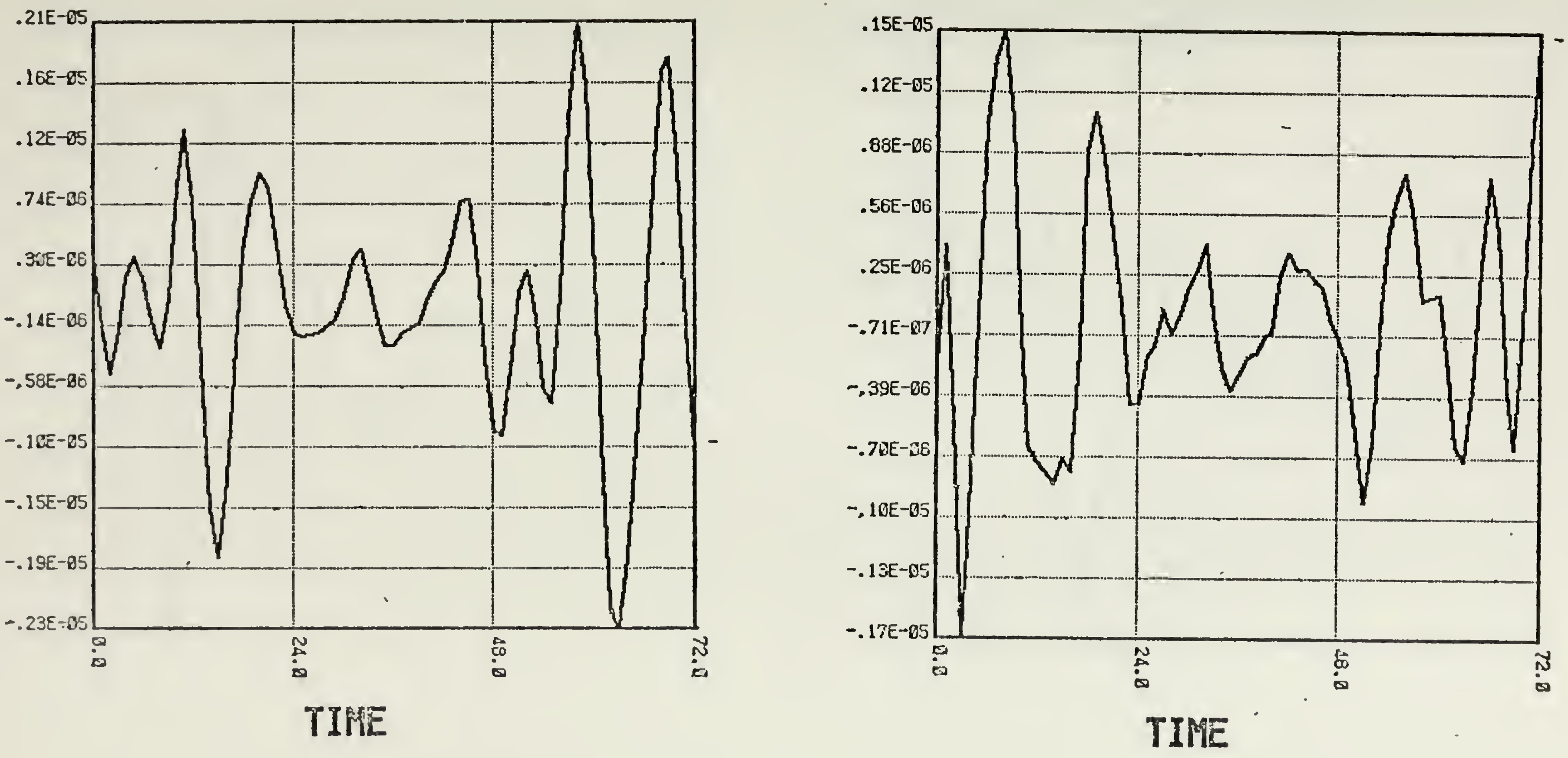

25a

25b

Figure 25. Gravity wave noise in the first interval mode - otherwise as in Fig. 24.

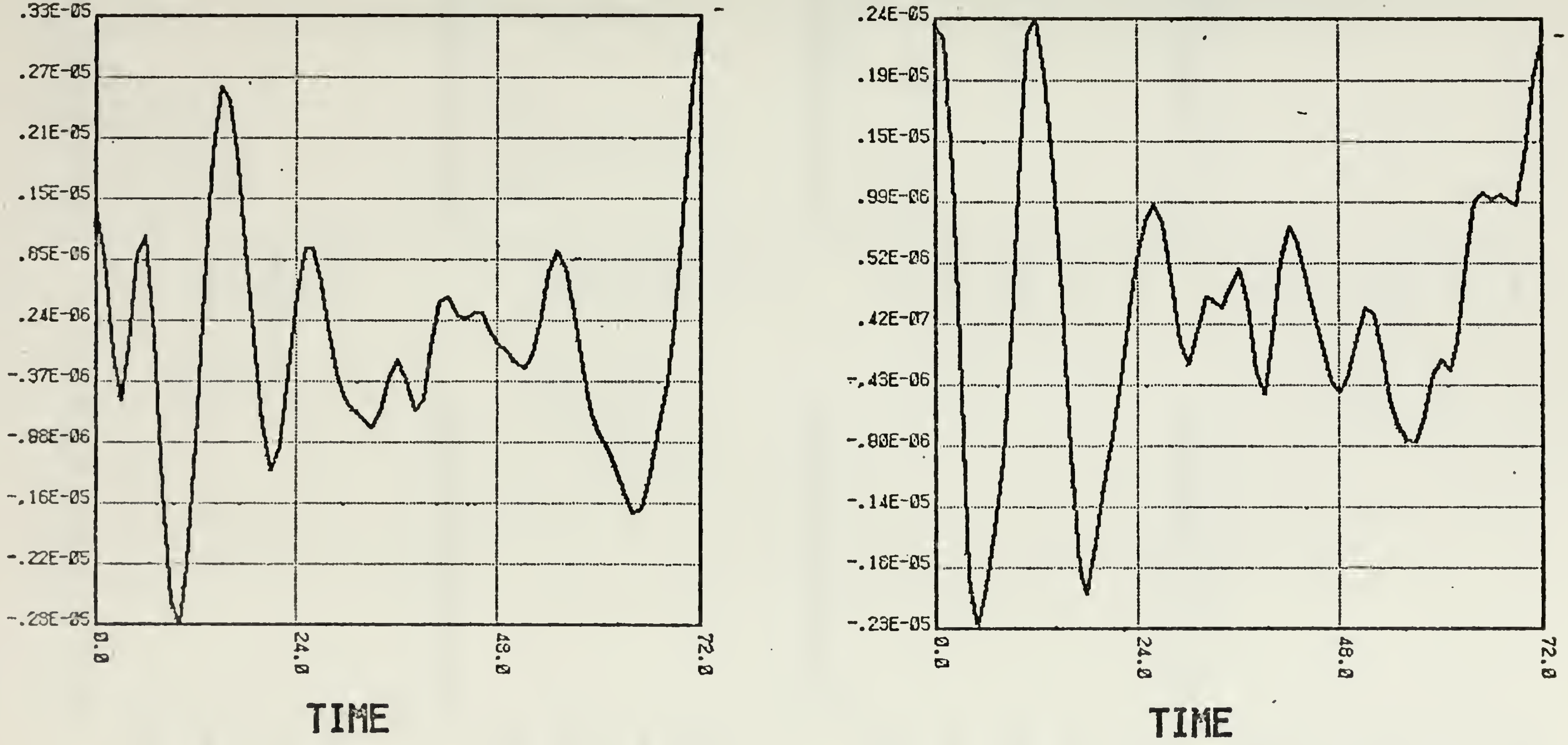

26a

26b

Figure 26. Gravity wave noise in the second interval - otherwise as in Fig. 24.

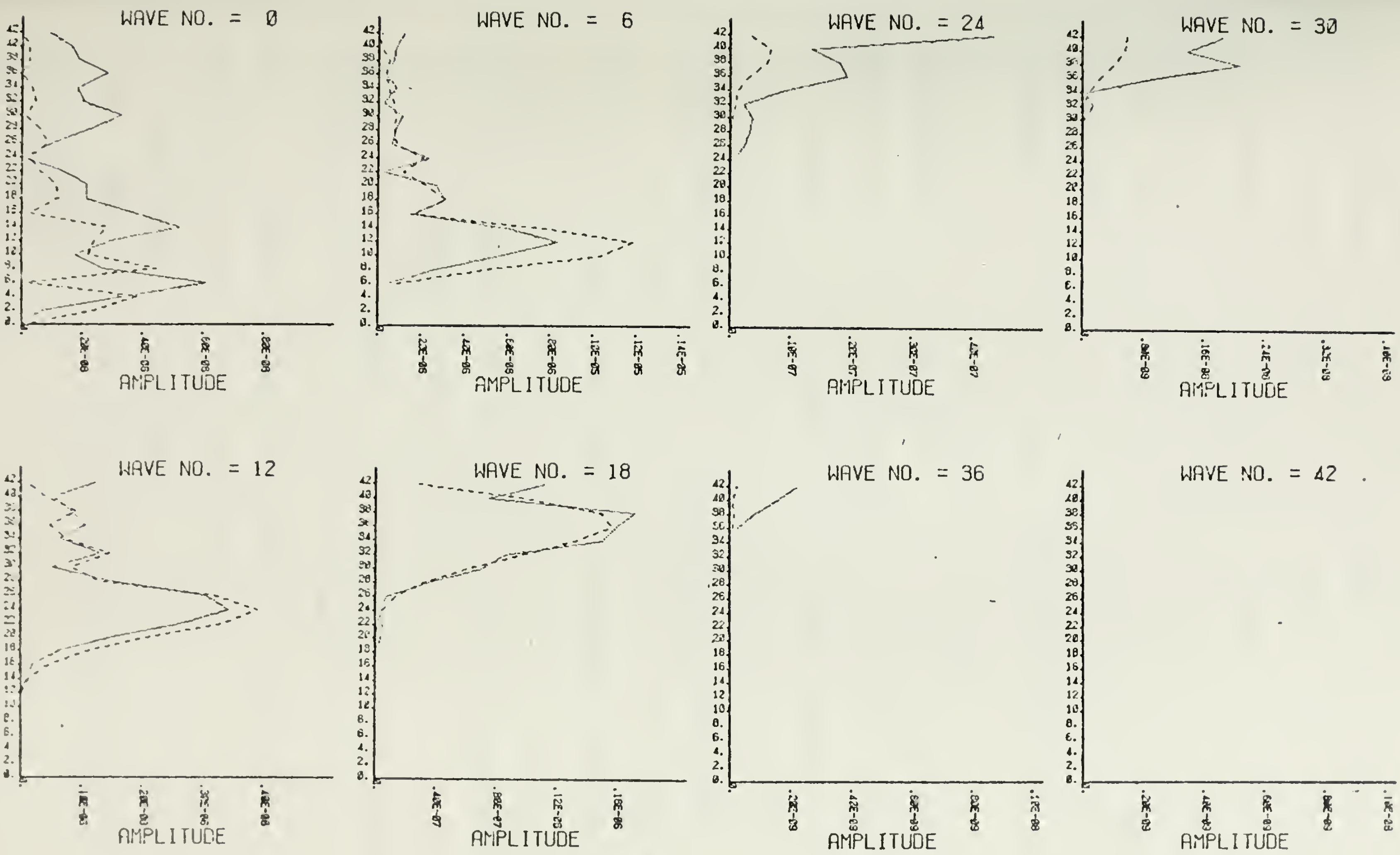

Figure 27. Initial divergence coefficients for the control case (dotted line) and Experiment B (dashed line). Vertical axis is latitudinal wave number (lat. index of the spherical harmonics). Horizontal scale is $\sec^{-1}$.

One motive for initializing with the quasi-geostrophic divergence is that, presumably, the "true" divergence would be approximated at the start and that the model would thus develop this divergence field earlier than a non-divergent initialization. Figures 28 and 29 address this point. They show that at 6 hours into the integrations, zonal wave numbers 6, 12, 18 do, in fact, approach the control divergence slightly faster. There is almost no difference for the higher wave numbers and the mean field shows poor adjustment in either case. This might be expected for the mean field since the geostrophic adjustment process is very inefficient at this scale in a bounded region. On the other hand, the higher wave numbers adjust very rapidly and after 6 hrs, they are in good agreement with the control case.

In light of the results showing good agreement in the initial quasi-geostrophic divergence with the control divergence for zonal wave number 6, 12, 18 and bad agreement for other scales, it is natural to modify Experiment B such that only scales corresponding to m = 6, 12, 18 are used in the quasi-geostrophic divergence. Figure 30 shows the time series of the external divergence mode for this experiment. Figure 31 shows the spectral adjustment of the divergence at 6 hours. The corresponding results for the unmodified Experiment B are Figs. 24 and 29. The results are almost identical to the unmodified quasi-geostrophic divergence results.

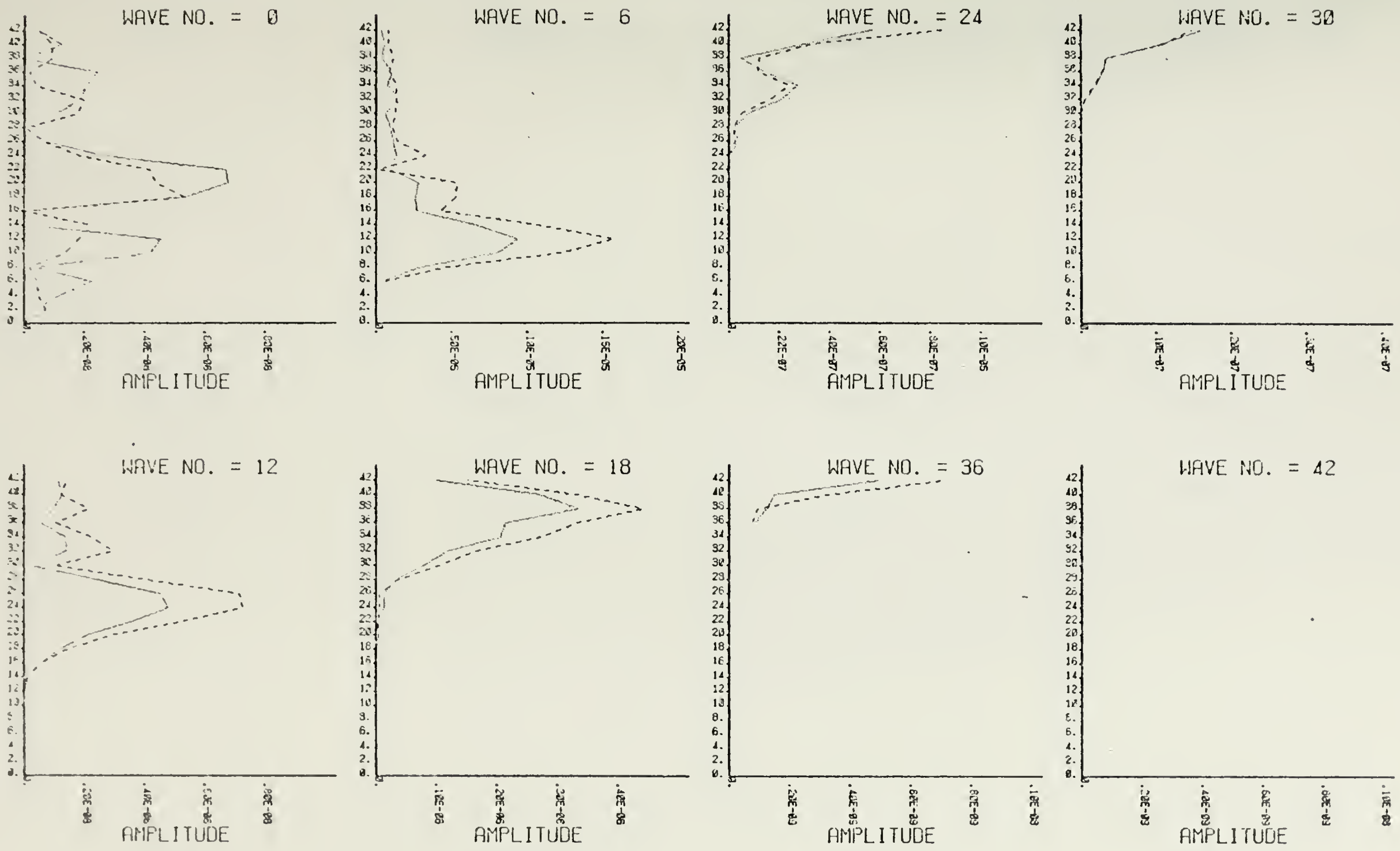

Figure 28. 6 hr divergence coefficients for the control case (dotted line) and Experiment A (dashed line) - otherwise as in Fig. 27.

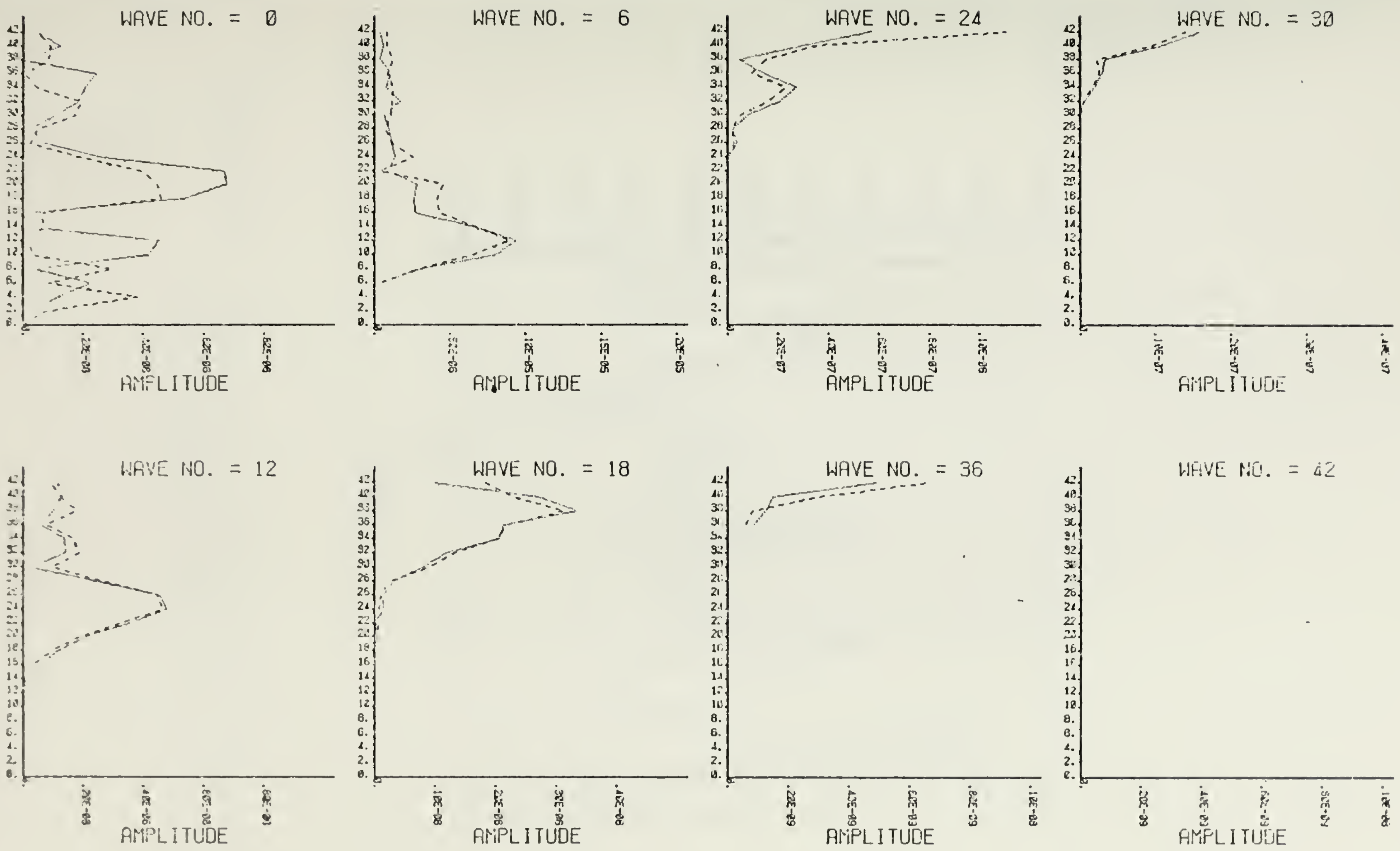

Figure 29. 6 hr divergence coefficients for the control case (dotted line) and Experiment B (dashed line) - otherwise as in Fig. 27.

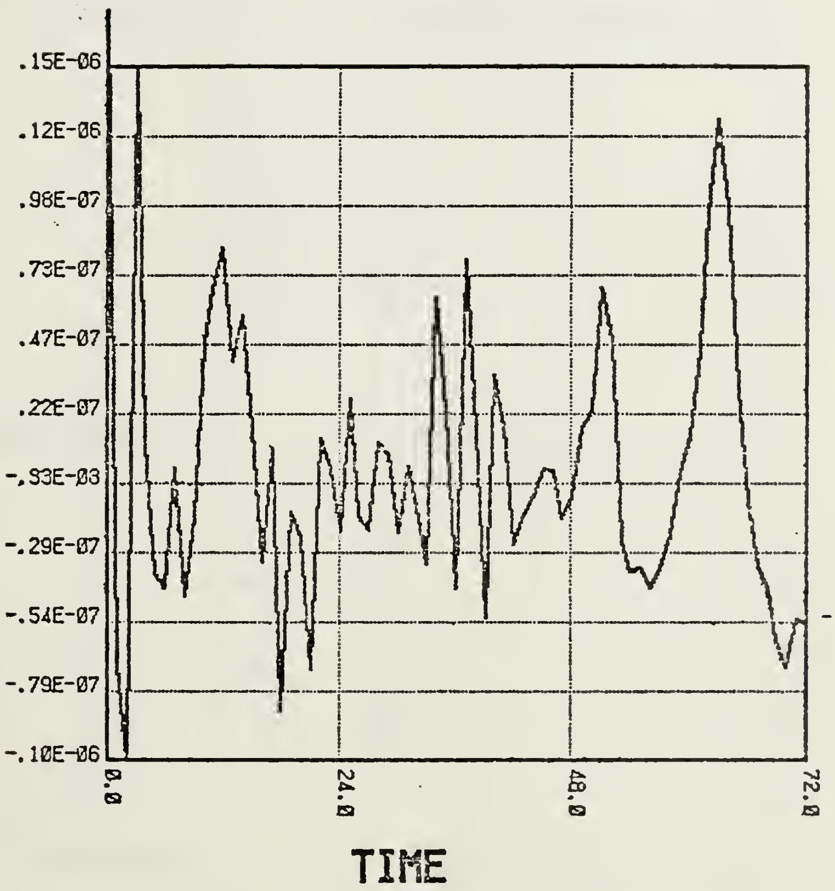

Figure 30. Time series of the gravity wave noise in the modified Experiment B. Vertical scale is $\sec^{-1}$. Time is in hrs.

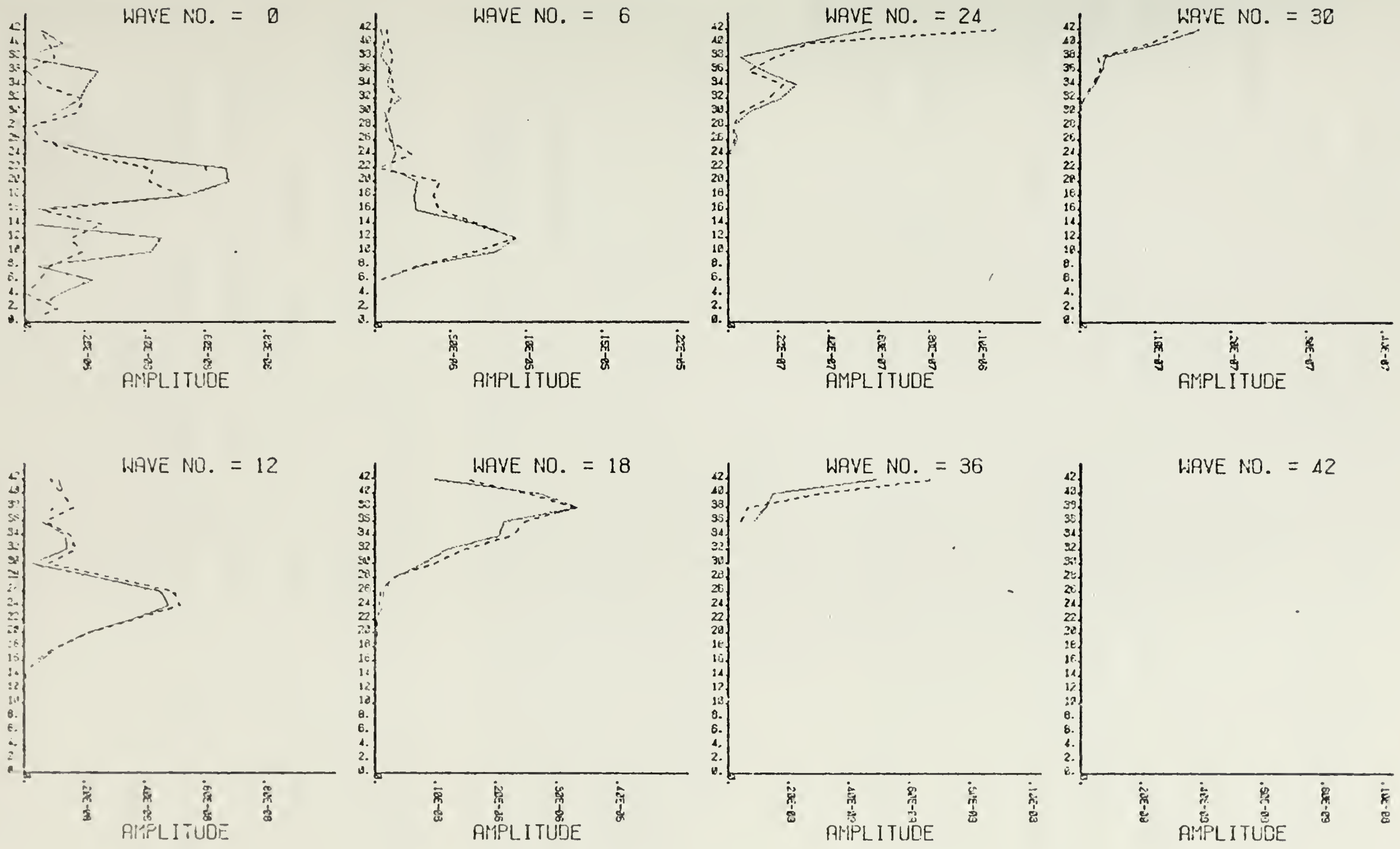

Figure 31. 6 hr divergence coefficients for the control case (dotted line) and modified Experiment B (dashed line). Vertical axis latitudinal wave no. Horizontal scale is sec^{-1}.

D. EXPERIMENT C

As discussed in Hoskins and Simmons (1975), a linear stability analysis of the semi-implicit scheme shows that the time step is limited only by the Rossby waves. The effect of the scheme is to slow down the faster moving gravity wave modes so that the integrations do not amplify in time. Slower moving atmospheric motions are less affected. Table II presents sample calculations of the distortion of the periods of the gravity waves present in these experiments for two time steps. These may be compared with Table I. The general behavior is that the periods increase with increasing time steps.

TABLE II

Δt	External	First	Second	Third	Fourth
12 mins	3.31	11.14	28.0	61.7	154.0
60 mins	5.7	12.2	28.5	61.9	154.1

Two points will be investigated in this experiment. The first is that the semi-implicit scheme should tend to smooth out high frequency oscillations, particularly with a large time step. The second is that the semi-implicit method might possibly hamper the geostrophic adjustment process since it slows down the gravity waves which are the mechanism for the adjustment.

Figure 32 shows the pressure tendencies using the semi-implicit method with time steps of 12 and 60 mins. Comparing this with the corresponding results for the explicit integrations (Fig. 19a), it is evident that the effect of the semi-implicit method is to smooth out the 3 hr oscillations. Figure 33 shows the relative effect of a small vs. large time step in the semi-implicit method on the external gravity waves. The larger period of the 60 min time step is evident. The larger time step initially amplifies the computational noise, but after 24 hrs it is considerably damped. The smoothing in the pressure tendencies is postulated to come about from the decreased velocity of the external gravity mode assuming an advective time scale.

The second point of this experiment is shown in Figs. 34 and 35. Comparison of the divergence coefficients for time steps of 12 and 60 mins shows no difference at 3 hrs. The adjustment of the divergence to the control case is apparently the same for either time step.

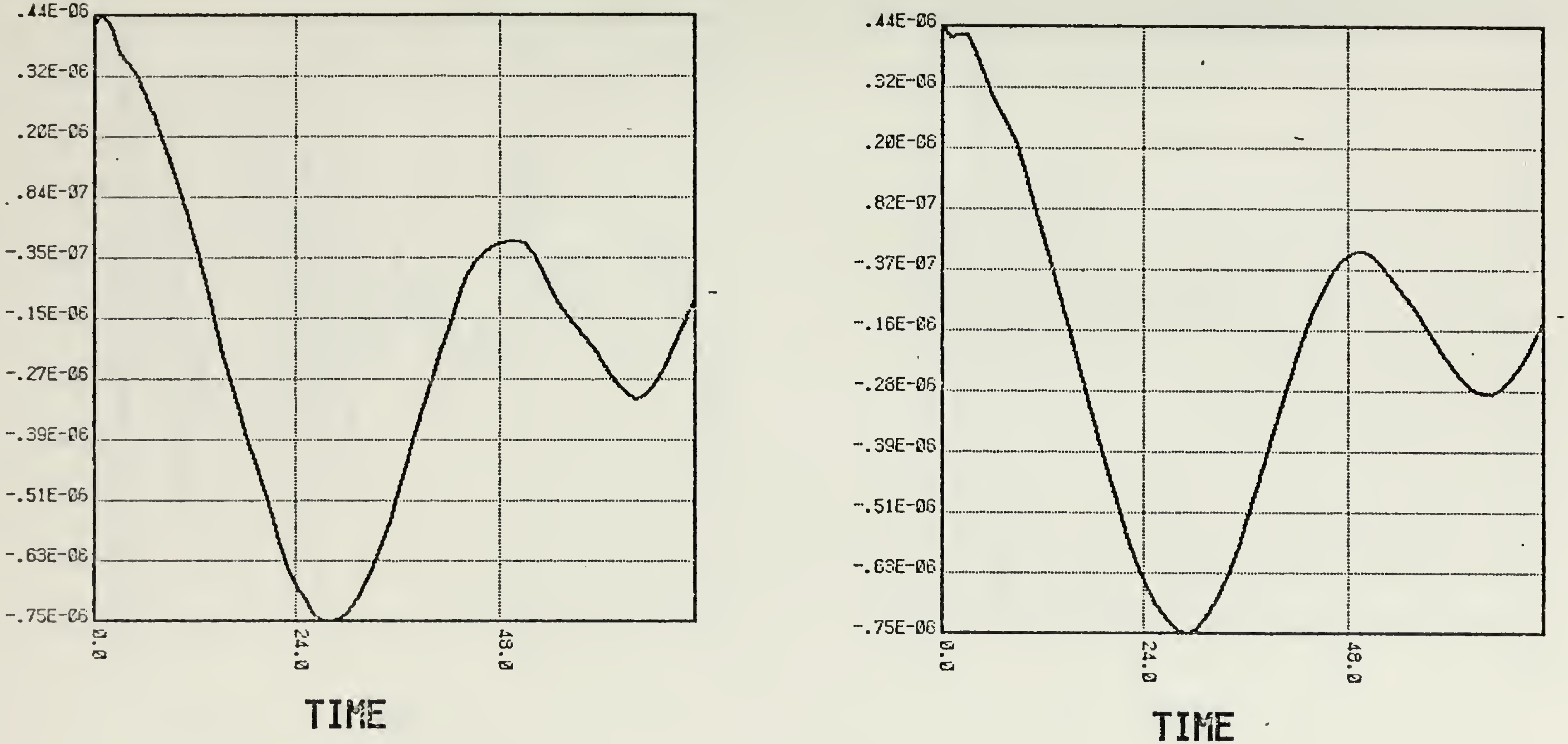

32a

32b

Figure 32. ∂q/∂t for Experiment C with a time step of 12 mins (32a) and 60 mins (32b). Vertical scale is sec^{-1}.

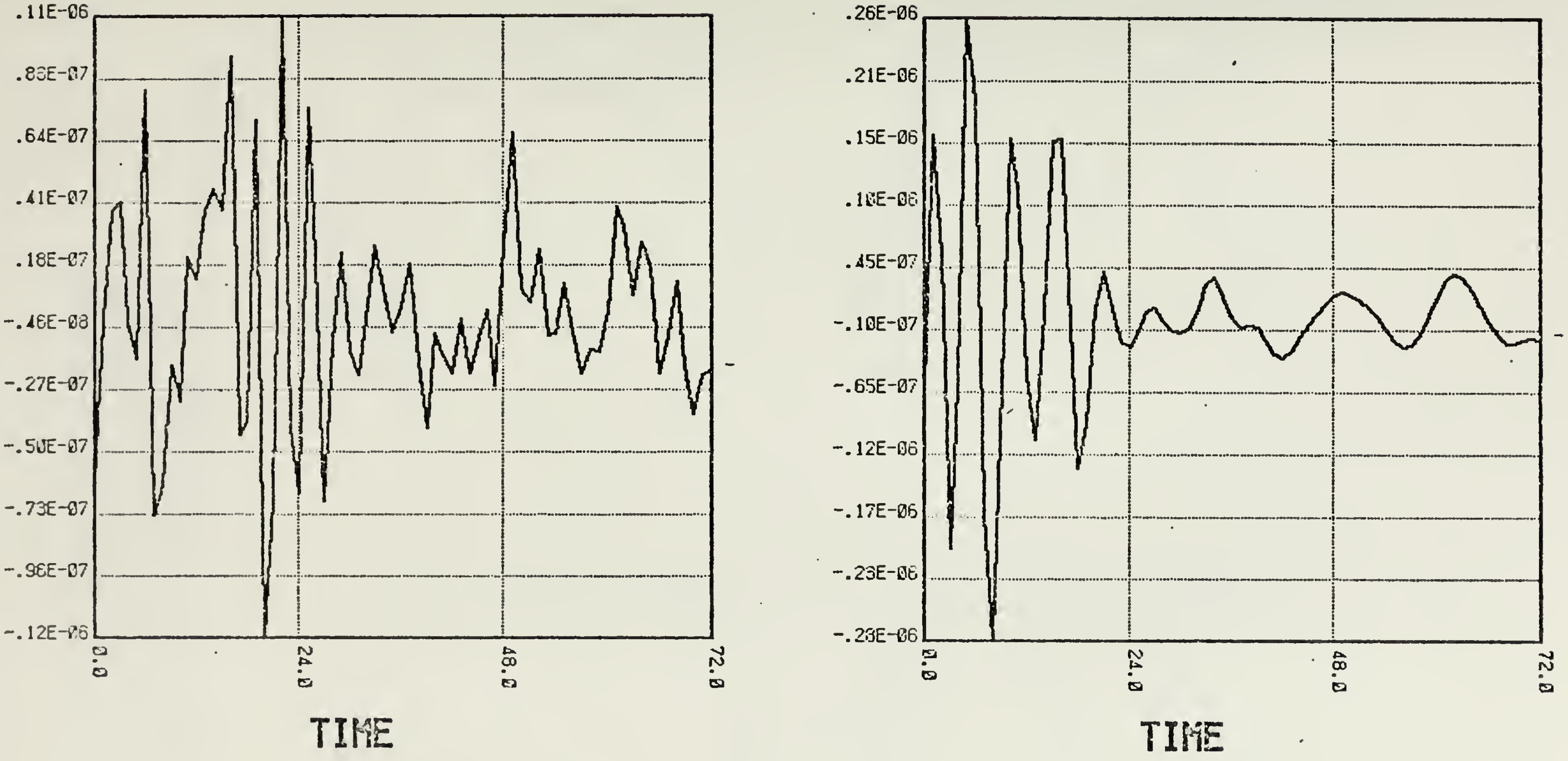

33a

33b

Figure 33. Gravity wave noise in the external mode for Experiment C with time steps of 12 mins (33a) and 60 mins (33b). Vertical scale is $\sec^{-1}$.

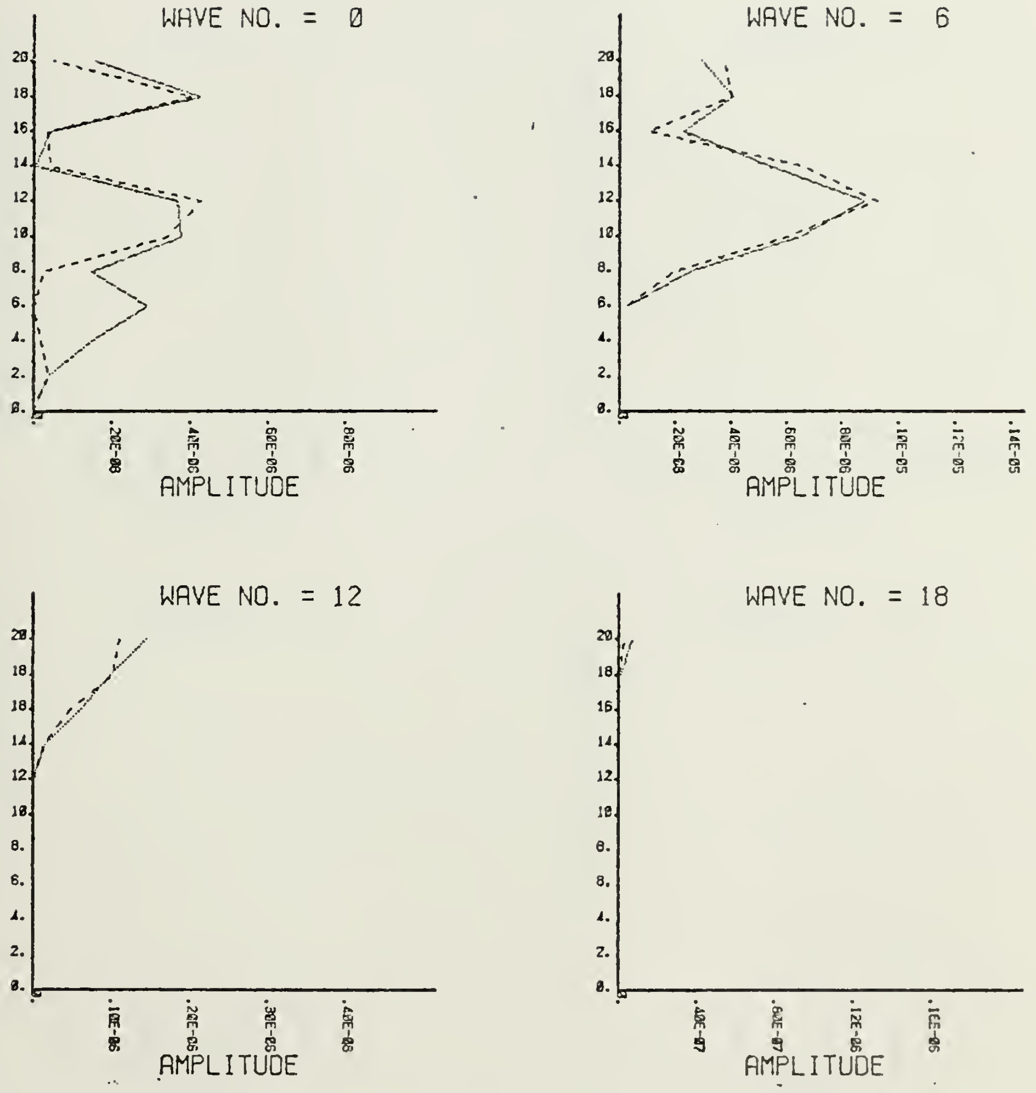

Figure 34. 3 hr divergence coefficients for the low resolution control case (dotted line) and Experiment C with a 12 min time step (dashed line). Vertical axis is latitudinal wave no. Horizontal scale is sec^{-1}.

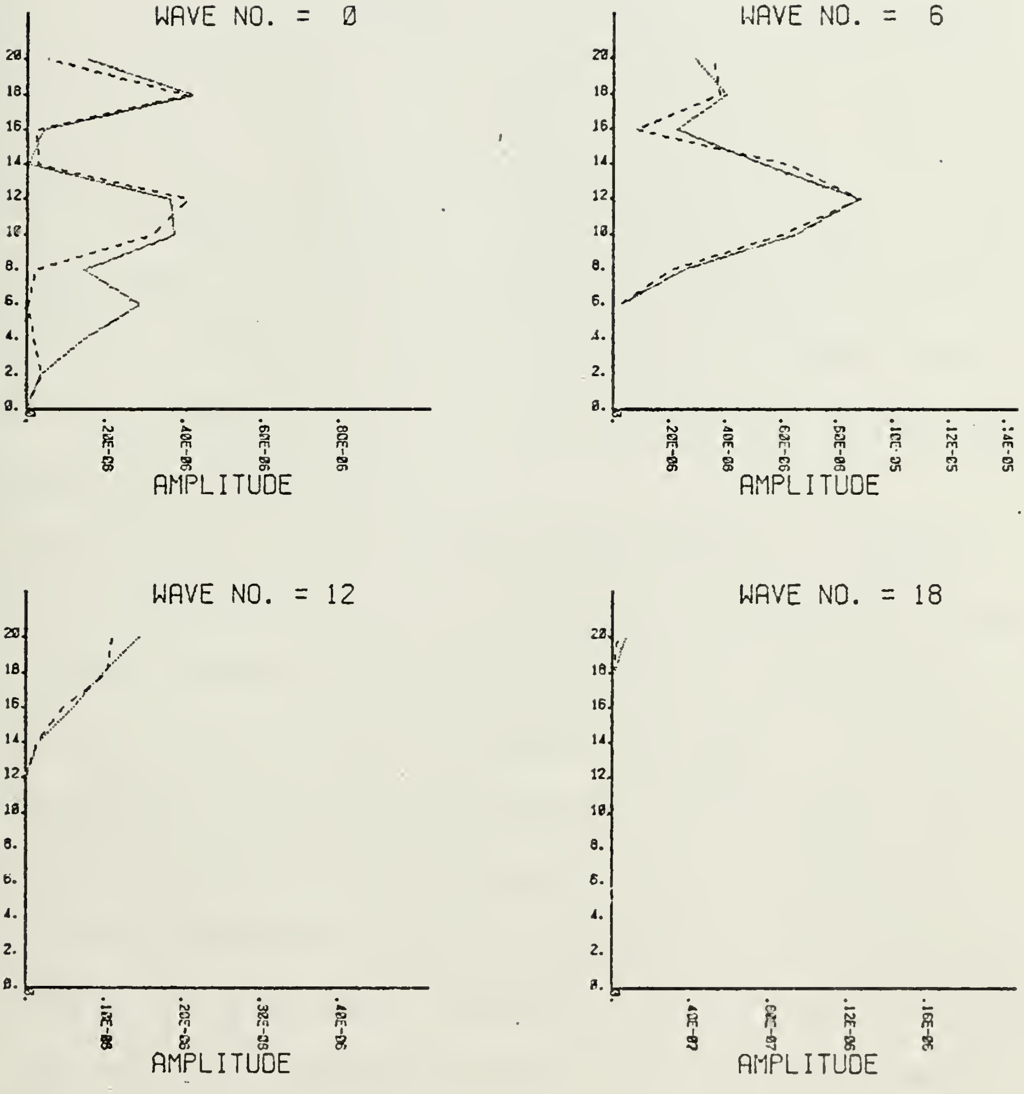

Figure 35. 3 hr divergence coefficients with a 60 min time step - otherwise as in Fig. 34.

VII. SUMMARY AND CONCLUSIONS

The results of this study are based upon the divergence developed by a baroclinic wave on a uniform earth. Initialization without the divergent wind component generated spurious inertial gravity waves. The internal state of the initial fields had nearly zero mean divergence. Thus, the external mode of the generated gravity waves was an order of magnitude less than the total divergence and was not significant. However, the internal gravity wave modes generated were significant. An important source for the external mode, namely topography, was neglected.

Initializing with the quasi-geostrophic divergence generally decreased the spurious gravity wave noise and aided the ensuing integrations to develop a divergence closer to the control case, but both effects were small. Furthermore, the advantage of the quasi-geostrophic divergence decreased when smaller scales were included in the integrations. Inserting the quasi-geostrophic divergence into only synoptic scales gave no advantage. However, the effect of this experiment may have been reduced by the fact that there were no planetary scale waves.

Using a semi-implicit scheme with the same time step as an explicit integration had no effect on the divergence modes but did smooth out oscillations in the pressure tendencies.

A larger time step initially increased the amplitude and period of the fast external gravity waves and had less effect on slower moving motions while still stabilizing pressure tendencies.

In general, the effect of a divergent initialization for a global primitive equation model is small. This same conclusion has been reached by two similar studies - Houghton et al (1971) and Dey et al (1975). This study, however, has neglected any physical processes such as precipitation as well as orography and the effect of an initial divergence in these cases may well be more important.

REFERENCES

Arakawa, A., and V. R. Lamb, 1976: Computational Design of the Basic Dynamical Processes of the UCLA General Circulation Model, 160 pp.

Bourke, W., 1974: A Multi-Level Spectral Model I. Formulation and Hemispheric Integrations. Mon. Wea. Rev., 102, 687-701.

Dey, C. H., J. A. Brown, and R. D. McPherson, 1975: Some Initialization Experiments with the NMC Global Model. The GARP Programme on Numerical Experimentation, Rpt. No. 8.

Hoskins, B. J. and A. J. Simmons, 1975: A Multi-Layer Spectral Model and the Semi-Implicit Method. Quart. J. Roy. Meteor. Soc., 101, 637-655.

Houghton, D., D. Baumhefner, and W. M. Washington, 1971: On Global Initialization of the Primitive Equations: Part II. The Divergent Component of the Horizontal Wind. J. Appl. Meteor., 10, 626-634.

Orszag, S. A., 1971: Numerical Simulation of Incompressible Flows within Simple Boundaries - Galerkin Spectral Representations. Studies in Appl. Math., Vol. L, 293-327.

Robert, A. J., J. Henderson and C. Turnbull, 1972: An Implicit Time Integration Scheme for Baroclinic Modes of the Atmosphere. Mon. Wea. Rev., 100, 329-335.

Simmons, A.J. and B. J. Hoskins, 1976: Baroclinic Instability on the Spheres: Normal Modes of the Primitive and Quasi-Geostrophic Equations. J. Atmos. Sci., 33, 1454-1477.

INITIAL DISTRIBUTION LIST

		No. Copies
1.	Defense Documentation Center Cameron Station Alexandria, Virginia 22314	2
2.	Library, Code 0142 Naval Postgraduate School Monterey, California 93940	2
3.	Dr. G. J. Haltiner, Code 63Ha Chairman, Department of Meteorology Naval Postgraduate School Monterey, California 93940	1
4.	Dr. R. T. Williams, Code 63Wu Department of Meteorology Naval Postgraduate School Monterey, California 93940	3
5.	Director Naval Oceanography and Meteorology National Space Technology Laboratories Bay St. Louis, Mississippi 39520	1
6.	Officer in Charge Navy Environmental Prediction Research Facility Monterey, California 93940	1
7.	Commanding Officer Fleet Numerical Weather Central Monterey, California 93940	1
8.	Dr. T. Rosmond Naval Environmental Prediction Research Facility Monterey, California 93940	2
9.	Lt. Olaf M. Lubeck COMNAVMARIANAS Box 12 FPO San Francisco 96630	3

Thesis
L885
c.1

Lubeck

171887

Divergent initialization experiments using a global primitive equation spectral model

DEC 17 85

33259

Thesis
L885
c.1

Lubeck

171887

Divergent initialization experiments using a global primitive equation spectral model.

thesL885
Divergent initialization experiments usi
3 2768 002 12382 0
DUDLEY KNOX LIBRARY